

# The Phase Diagram of QC<sub>2</sub>D from Functional Methods

Naseemuddin Khan,<sup>1,2</sup> Jan M. Pawłowski,<sup>1,2</sup> Fabian Rennecke,<sup>3</sup> and Michael M. Scherer<sup>1</sup>

<sup>1</sup>*Institut für Theoretische Physik, Heidelberg University, Philosophenweg 16, 62910 Heidelberg, Germany*

<sup>2</sup>*ExtreMe Matter Institute EMMI, GSI Helmholtzzentrum für Schwerionenforschung, Planckstr. 1, 64291 Darmstadt, Germany*

<sup>3</sup>*Institut für Theoretische Physik, Justus-Liebig-Universität Gießen, Heinrich-Buff-Ring 16, 35392 Gießen, Germany*

We study the phase diagram of two-color Quantum Chromodynamics at finite temperature and chemical potential. This is done within an effective low-energy description in terms of quarks, mesons and diquarks. Quantum, thermal and density fluctuations are taken into account with the functional renormalisation group approach. In particular, we establish the phenomenon of pre-condensation, affecting the location of the phase boundary to Bose-Einstein condensation. We also discuss the Silver Blaze property in the context of the functional renormalisation group.

PACS numbers: 05.10.Cc, 11.10.Wx, 12.38.Aw

## I. INTRODUCTION

The investigation of the phase diagram of Quantum Chromodynamics (QCD) at finite temperature and density is an area of very active experimental and theoretical research [1]. So far, theoretical investigations of the QCD phase structure have not matured enough to provide quantitative predictions at finite density. While ab initio lattice simulations at finite density are hampered by the sign problem, ab initio continuum computations are hampered by the so far missing access to all fluctuating degrees of freedom at high density. Moreover, at high density we also expect competing order effects that further increase the need for fully quantitative computations. In this situation the investigation of QCD-like theories, that lack the above-mentioned problems, is an interesting option for shedding light on particular aspects of finite density QCD. In the present work we study QCD with two colors,  $N_c = 2$ , and two quark flavors  $N_f = 2$ . Two-color QCD (QC<sub>2</sub>D) has no sign problem, and exhibits an additional meson-baryon symmetry (Pauli-Gürsey) not present in QCD with three colors. In QC<sub>2</sub>D baryons are diquark states and the meson-baryon symmetry is related to the bosonic nature of the baryons. Consequently QC<sub>2</sub>D allows for both, the chirally broken mesonic phase of quark-antiquark pairs known from QCD, and the (Bose-Einstein-) condensation of colorless diquarks. In summary, despite its qualitative difference to QCD, QC<sub>2</sub>D also shares many interesting similarities with QCD. Moreover, its accessibility for lattice simulations makes it a perfect testbed for continuum approaches to QCD, both for ab initio computations and low-energy effective theories.

For the above reasons QC<sub>2</sub>D has recently attracted strong interest. It has been studied within mean field theory and the chiral Lagrangian approach [2–9], random matrix models [10] and within Nambu–Jona-Lasinio-type models [11–20]. For an even number of quark flavors  $N_f$  the SU(2) gauge group provides a positive path integral measure and thus avoids the occurrence of a fermion-sign problem. This facilitates the investigation of the QC<sub>2</sub>D phase diagram by lattice simulations [21–32].

In this work we employ the functional renormalisation

group (FRG) approach to the quark-meson-diquark model, [33], to study the phase diagram of two-color QCD. For QCD-related reviews of the FRG see [34–43]. In the case of QC<sub>2</sub>D a comprehensible FRG phase diagram for finite temperature and density has previously been established by Strodthoff *et al.* in Refs. [33, 44]. There, the flow equation for the effective potential was solved in the lowest order of the derivative expansion. Such an approximation takes into account momentum scale dependent multi-scattering processes of mesons and baryons.

In the present work we significantly extend the truncation scheme in [33, 44] by including non-perturbative corrections to the classical dispersion relations of quarks, mesons and diquarks by means of the respective running wave function renormalisations. We also take into account the momentum scale dependence of quark-meson and quark-diquark scattering processes with running Yukawa couplings. It has been shown in QCD as well as in the non-relativistic analogue of QC<sub>2</sub>D, namely the non-relativistic BCS-BEC crossover, that these fluctuations play a large quantitative rôle. For FRG work on this topic see e.g. [45–52], for reviews see [50, 51]. Here, we discuss their impact on the phase structure of QC<sub>2</sub>D. This includes a careful assessment of the Silver Blaze property. The latter is evaluated in the context of renormalisation group flows. We also deduce the basic requirements that approximations of  $n$ -point functions have to fulfil in order to maintain the Silver Blaze property. Finally, we also study pre-condensation in two-color QCD: This phenomenon can appear when a physics system in the disorder phase is close to a transition toward an ordered state. Pre-condensation means that order occurs at intermediate length scales or momentum scales. In the present FRG setting this phenomenon is easily accessible due to the successive integration of momentum modes. In summary we establish a refined picture of the FRG phase diagram for QC<sub>2</sub>D.

The paper is organised as follows: In Sec. II, we introduce the quark-meson diquark (QMD) model as a low energy effective theory for QC<sub>2</sub>D. In Sec. IIB, we review basics of the FRG method and discuss the Silver Blaze property in the present context, cf. Sec. IIC. We further discuss the truncation for the fluctuation analysis of the QMD-model, and derive the flow equations for the

effective potential, the wave function renormalisations and the Yukawa couplings in Sec. III. The results for the chiral and diquark condensation and related phase diagrams are presented in Sec. IV, and are compared to the literature. Technical details as well as an analysis of truncation effects are given in the Appendix.

## II. LOW-ENERGY DESCRIPTION OF QC<sub>2</sub>D

Here we outline the construction of our low-energy description of QC<sub>2</sub>D with two quark flavors. By integrating out the gluons first, we derive a low energy effective model in terms of quarks, mesons and diquarks, [33], valid at momentum- or energy scales  $\Lambda \lesssim 1$  GeV. The quantum, thermal and density fluctuations below  $\Lambda$  are taken into account within the functional renormalisation group approach.

### A. Quark-Meson-Diquark Model for QC<sub>2</sub>D

The starting point is the microscopic QCD Lagrangian. Here we focus on the matter part,

$$\mathcal{L}_{\text{mat}} = q_L^\dagger i\sigma_\mu D_\mu q_L + q_R^\dagger i\sigma_\mu^\dagger D_\mu q_R + im_q \bar{q}q, \quad (1)$$

where the covariant derivative  $D_\mu = \partial_\mu + igA_\mu$  couples quarks to gluons via the strong coupling  $g$ , where  $A_\mu = A_\mu^a t_a$  with the gauge group generators  $t_a$ . We define  $\sigma_\mu = (i\sigma_j, \mathbb{1})$  with the Pauli matrices  $\sigma_j$ . The  $\gamma$ -matrices are defined as

$$\gamma_j = \begin{pmatrix} 0 & -i\sigma_j \\ i\sigma_j & 0 \end{pmatrix}, \quad \gamma_0 = \begin{pmatrix} 0 & \mathbb{1} \\ \mathbb{1} & 0 \end{pmatrix}, \quad \gamma_5 = \begin{pmatrix} \mathbb{1} & 0 \\ 0 & -\mathbb{1} \end{pmatrix}. \quad (2)$$

In the case of two colors, the gauge group generators (the Pauli matrices) are pseudo-real,  $t_a^* = t_a^T = -t_a t_a$ . This property leads to an extended  $SU(2N_f)$  flavor symmetry, also known as Pauli-Gürsey symmetry. Naturally, various four-fermion interaction channels are generated by gluon-exchange diagrams, cf. Fig. 1. In the present low energy effective model we allow for interaction terms respecting the  $SU(4)$  flavor symmetry of QC<sub>2</sub>D with a scalar, a pseudo-scalar and a diquark channel. Basically, this is a minimal two-flavor Nambu-Jona-Lasinio (NJL) Lagrangian, supplemented with a diquark term,

$$\begin{aligned} \mathcal{L}_{\text{NJL}} = & \mathcal{L}_{\text{kin}}^q + \lambda_q [(\bar{q}q)^2 + (\bar{q}i\gamma_5\vec{\tau}q)^2 \\ & + (\bar{q}i\gamma_5\tau_2 t_2 C \bar{q}^T)(q^T C i\gamma_5\tau_2 t_2 q)], \end{aligned} \quad (3)$$

where  $C = \gamma_2\gamma_0$  is the charge conjugation operator and the  $\tau_i$ 's are Pauli matrices in flavor (isospin) space. The coupling constants for the various channels are fixed by the  $SU(4)$  flavor symmetry. The low-energy properties of QC<sub>2</sub>D can be described most efficiently by composite fields obtained with a Hubbard-Stratonovich transformations. For the NJL model with the interaction Lagrangian in (3) this amounts to the introduction of

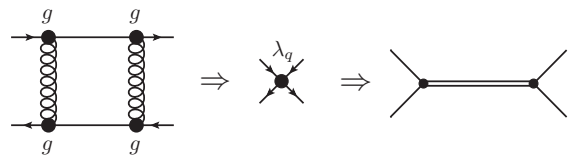


Figure 1: An effective four-fermi coupling (middle) is generated by gluon exchange (left). This process is the starting point to motivate effective models, where high energy degrees of freedom have been integrated out. By means of a Hubbard-Stratonovich transformation we introduce composite fields into our model as, e.g., represented by the double line in the diagram on the right.

a meson field  $\phi = (\vec{\pi}, \sigma)$  which parametrises the pairing in the pseudo-scalar and the scalar channel as well as a complex diquark field  $\Delta$ . A fluctuation analysis of the above action leads to a propagation of the meson and diquark degrees of freedom, represented by kinetic terms of mesons and diquarks as well as a regeneration of four-fermi interactions. The latter can be rewritten as corrections of the propagators and vertices of quarks and composite fields leading to vanishing meson and diquark channels of the four-fermi interaction at all cutoff scales. This dynamical hadronisation, [37, 53, 54], has been detailed in QCD in [55, 56]. In the present work we neglect the related effects that is in particular important for the high density part of the phase diagram, for a discussion see [43].

For the investigation of the theory at finite density a coupling to a chemical potential  $\mu$  for the quarks as well as for the diquarks has to be included. Putting everything together we are led to the Lagrangian of the QMD-model,

$$\begin{aligned} \mathcal{L}_{\text{QMD}} = & \bar{q} (i\not{\partial} + i\gamma_0\mu + ih(\sigma + i\gamma_5\vec{\tau} \cdot \vec{\pi})) q \\ & + \frac{1}{2}m^2 (\vec{\pi}^2 + \sigma^2 + |\Delta|^2) - c\sigma \\ & + \frac{h}{2} (i\Delta^* q^T C \gamma_5 \tau_2 t_2 q - \text{h.c.}) \\ & + \frac{1}{2}(\partial_\mu \vec{\pi})^2 + \frac{1}{2}(\partial_\mu \sigma)^2 + \frac{1}{2} |\partial_i \Delta|^2 \\ & + \frac{1}{2} (\partial_\tau - 2\mu) \Delta^* (\partial_\tau + 2\mu) \Delta. \end{aligned} \quad (4)$$

The four-fermi interaction in (3) is turned into a Yukawa-interaction  $h$  between quarks, mesons and diquarks. In such a low-energy effective theory, the gluon fields are considered to be integrated out. This approach is supported by the mass gap in QCD which suppresses gluon fluctuations for low momentum scales. This is most easily seen in the Landau gauge where the QCD mass gap translates in a mass gap in the gluon propagator. Since the mass gap of the gluon is of the order of 1 GeV, the UV-cutoff of our model has to be chosen accordingly, i.e.  $\Lambda \approx 1$  GeV.

Figure 2: RG flow of the effective action of the Quark-Meson-Diquark model (QMD). The meson, diquark and quark propagators are represented by dashed, double and solid lines respectively. The filled circles indicate that these are the full propagators. The crosses denote the regulator insertion  $\partial_t R_k$ .

## B. Functional Renormalisation

For our study of the phase diagram of the quark-meson-diquark (QMD) model we use the functional renormalisation group (FRG) approach. The FRG is formulated as a functional differential equation for the scale-dependent effective action or free energy  $\Gamma_k$ . Its scale dependence is governed by the Wetterich equation, [57],

$$\partial_t \Gamma_k[\Phi] = \frac{1}{2} \text{Tr} G_k[\phi] \partial_t R_k, \quad t = \log k/\Lambda, \quad (5)$$

with some reference scale  $\Lambda$ , typically the initial UV scale, and  $G_k[\Phi]$  is the full field-dependent propagator,

$$G_k[\phi] = \frac{1}{\Gamma_k^{(2)}[\Phi] + R_k}, \quad \Gamma_k^{(2)} = \frac{\delta^2 \Gamma_k}{\delta \Phi^2}. \quad (6)$$

In (5), (6), the field  $\Phi$  collects all bosonic and fermionic degrees of freedom of the model. The trace in (5) contains a sum over internal indices with a relative minus sign for fermions as well as a momentum integration. The function  $R_k = R_k(q)$  acts as a momentum-dependent mass, suppressing infrared modes below the RG scale  $k$  and leaving the UV unchanged. The solution to (5) provides a renormalisation group trajectory, interpolating between the microscopic action  $\Gamma_\Lambda$  at the ultraviolet scale  $\Lambda$  and the full quantum effective action  $\Gamma = \Gamma_{k \rightarrow 0}$ .

The flow equation (5) is a functional integro-differential equation which only in rare cases admits a full solution. In most cases one has to resort to approximations of the full effective action. For a discussion of suitable approximation schemes and their convergence we refer to the extensive literature, for QCD-related reviews see [34–43].

In the present work we use the QMD model (4), [33], as derived in the previous section. The flow equation for the effective action is depicted diagrammatically in Fig. 2. It comprises quantum, thermal and density fluctuations of quarks, mesons and diquarks. The approximation scheme used in the present work is discussed in Sec. III.

## C. Silver Blaze Property

At vanishing temperature the quark chemical potential  $\mu$  has to exceed a critical value  $\mu_c = m_{\Delta, \text{pol}}/2$ , before a finite density can be reached. Here,  $m_{\Delta, \text{pol}}$  is the pole

mass of the diquark, which is the lowest lying state with non-vanishing baryon number. For  $\mu > \mu_c$ , diquarks can be generated leading to a finite density. For  $\mu < \mu_c$  the density is vanishing. The  $\mu$  independence below the onset chemical potential  $\mu_c$  of the density translates to a trivial one for all correlation functions in QC<sub>2</sub>D, see (7) and below, and also holds in QCD with  $\mu_c = m_{\text{baryon, pol}}/3$ . It is related to the pole- and cut-structure of the correlation functions in momentum space, and is called the *Silver Blaze property* [58].

For 1PI correlation functions  $\Gamma_k^{(n)}$  in the presence of a regulator the Silver Blaze property reads schematically

$$\Gamma_k^{(n)}(p_1, \dots, p_n; \mu) = \Gamma_k^{(n)}(\tilde{p}_1, \dots, \tilde{p}_n; 0), \quad \mu < \mu_c, \quad (7)$$

with

$$\Gamma_k^{(n)} = \frac{\delta^n \Gamma_k}{\delta \Phi^n}, \quad \tilde{p}_i = (p_{i0} + i c_i \mu, \vec{p}_i), \quad (8)$$

and  $c_i/2$  is the baryon number of the field  $\Phi_i$  in QC<sub>2</sub>D. In QCD this translates into  $c_i/3$  which reflects three colors. Eq. (7) requires regulators with

$$R_k(p; \mu) = R_k(\tilde{p}; 0). \quad (9)$$

Moreover,  $R_k$  should not lower the pole mass of the lowest lying state with non-vanishing baryon number. Note that (7) and (9) implies the same property for the propagator,

$$G_k(p_1, p_2; \mu) = G_k(\tilde{p}_1, \tilde{p}_2; 0), \quad \mu < \mu_c. \quad (10)$$

At  $k=0$ , (7) is the standard Silver-blaze property, see [59] for a recent lucid diagrammatic proof within the 2PI-approach.

In summary (7) entails that below the critical or onset chemical potential,  $\mu_c$ , the  $\mu$ -dependence of the  $n$ -point functions is that of the frequency arguments,  $p_i \rightarrow \tilde{p}_i$ . This also makes clear why the onset chemical potential is given by the pole mass of the lowest lying state with non-vanishing baryon number: the pole mass of, e.g. the diquark, is given by the condition

$$\Gamma_{k, \Delta}^{(2)}(p^2 = -m_{\Delta, \text{pol}, \mu}^2; \mu) = 0, \quad \vec{p} = 0, \quad (11)$$

where  $m_{\Delta, \text{pol}, \mu}$  is the pole mass at finite  $\mu$ . As  $\Gamma_{k, \Delta}^{(2)}$  has the Silver Blaze property (7), this also holds for  $\Gamma_{k, \Delta}^{(2)}(\tilde{p}^2 = -m_{\Delta, \text{pol}}^2; 0)$  with the pole mass  $m_{\Delta, \text{pol}}$  at vanishing  $\mu$ . Eq. (11) is fulfilled for  $\tilde{p}^2 = -m_{\Delta, \text{pol}}^2$  which implies  $p^2 = 0$  and  $\mu = \mu_c = m_{\Delta, \text{pol}}/2$ . Hence, onset chemical potential and pole mass at vanishing  $\mu$  are the same due to the Silver blaze property. Note that this also implies that the pole mass at the critical chemical potential vanishes,  $m_{\Delta, \text{pol}, \mu_c} = 0$ . Moreover, at  $\mu_c$  the curvature mass,  $\Gamma_{k, \Delta}^{(2)}(p^2 = 0)$ , vanishes as well.

Note in this context that the curvature masses, e.g.  $\Gamma_{k, \Delta}^{(2)}(p^2 = 0)$  are not necessarily identical with the pole masses for all  $\mu$ . However, it has been observed in [60]

within the quark-meson model that this non-trivial relation holds well if fully momentum-dependent propagators are taken into account. In turn it fails in the local potential approximation. Additionally, it has been shown in [60] that the inclusion of wave function renormalisations  $Z_{k,\Phi}$  takes account of most of the momentum dependence and hence the non-trivial relation between pole and curvature mass is fulfilled with high accuracy. Thus, in the present work we account for the non-trivial momentum dependence of the two-point functions by the inclusion of running  $Z_{q/\phi/\Delta}$ .

The Silver blaze property also has important consequences for approximation schemes of the effective action: in order to retain the Silver Blaze property within a truncation, the frequency-dependence of the  $n$ -point functions relating to fields with non-vanishing baryon number has to be taken into account properly, see also [61]. Alternatively one may expand the correlation functions at  $\tilde{p}_i = 0$  with  $\tilde{p}$  in (8). In the present truncation this concerns the wave function renormalisations of quarks and diquarks, the Yukawa couplings as well as the diquark couplings in the effective potential, and will be discussed in Sec. III.

### 1. Silver Blaze Property from the functional RG

We proceed by showing the Silver Blaze property (7) with the help of the FRG. The FRG allows for a particularly simple proof due to its one-loop complete structure. The successive or iterative nature of the flow gives access to an inductive proof, which structurally works in the following way: we show that the flow of the correlation functions at some scale  $k$  has the Silver blaze property (7) if the correlation functions at this scale  $k$  have it. Hence, if the Silver Blaze property holds at one scale, it holds at every scale. In fact, due to asymptotic freedom, QC<sub>2</sub>D approaches the classical action at asymptotically large scales. In this case, the only momentum-dependent  $n$ -point function in QC<sub>2</sub>D is the two-point function of the quarks for which (7) holds. This leads to a classical or initial effective action for the QMD model which also has the Silver blaze property, see (4).

It is left to show that Silver Blaze holds for the flows  $\partial_t \Gamma_k^{(n)}$  provided that it holds for all  $\Gamma_k^{(n)}$ . We illustrate the structure of the proof at the example of the bosonic two-point function in a vanishing background,  $\Phi = 0$ . Furthermore, for the sake of simplicity we drop the quark contribution, effectively restricting ourselves to the purely bosonic sector of the theory. In a vanishing background the correlation function is diagonal in momentum space,  $\Gamma_k^{(2)}(p_1, p_2; \mu) \simeq \Gamma_k^{(2)}(p; \mu)$  times momentum conservation. This simplifies the flow, to wit

$$\begin{aligned} \partial_t \Gamma_k^{(2)}(p; \mu) = & -\frac{1}{2} \int_q \Gamma_k^{(4)}(p, q; \mu) \\ & \times G_k(q; \mu) \partial_t R_k(q; \mu) G_k(q; \mu), \end{aligned} \quad (12)$$

where we have used that the propagator as well as the

four-point function only depend on one and two momenta respectively. Now we utilise the assumption that the correlation functions at the scale  $k$  satisfy (7), which requires regulators with (9) and implies (10). In summary this leads to

$$\begin{aligned} \partial_t \Gamma_k^{(2)}(p; \mu) = & -\frac{1}{2} \int_{\tilde{q}} \Gamma_k^{(4)}(\tilde{p}, \tilde{q}; 0) \\ & \times G_k(\tilde{q}; 0) \partial_t R_k(\tilde{q}; 0) G_k(\tilde{q}; 0), \end{aligned} \quad (13)$$

where we have shifted the frequency integration over real  $q_0$  to one over  $q_0 + i\mu$ . This is possible as long as the integrand has no poles in the frequency integration contour given by  $q_0, q_0 + i\mu$  and the connecting lines at  $\pm\infty + iy$  with  $y \in [0, \mu]$ . For  $\mu < \mu_c$  all poles are at larger imaginary frequency values for all spatial momenta. Hence, the right hand side of (13) only depends on  $\mu$  via  $\tilde{p}$  and we conclude

$$\partial_t \Gamma_k^{(2)}(p; \mu) = \partial_t \Gamma_k^{(2)}(\tilde{p}; 0). \quad (14)$$

The one line proof from (12) to (13) extends trivially to the flow equation for  $\Gamma_k^{(2)}$  of our complete model including quark contributions, non-trivial background fields, and all higher correlation functions,  $\partial_t \Gamma_k^{(n)}$ : all diagrams have the same one-loop structure as (12), the difference only being a different number of vertices and propagators. Hence, the substitution of the vertices and propagators according to (7), (10) works similarly. The shift of all integrations  $q_i \rightarrow \tilde{q}_i$  is possible by the lack of poles between  $q_{0_i} \rightarrow q_{0_i} + i\mu$  for  $\mu < \mu_c$ . This leads us finally to

$$\partial_t \Gamma_k^{(n)}(p_1, \dots, p_n; \mu) = \partial_t \Gamma_k^{(n)}(\tilde{p}_1, \dots, \tilde{p}_n; 0). \quad (15)$$

We emphasise again that it is the one-loop structure of the flow that simplifies the proof.

## III. SET-UP AND FLOW EQUATIONS

Here we specify and discuss the truncation of the effective action we use in this work. The flow of the cutoff-dependent parameters are then extracted from the flow equation (5) for the effective action by appropriate projections which is also discussed in detail.

### A. Scale-dependent effective action

We promote all parameters of the QMD Lagrangian (4) to cutoff-scale dependent ones. In order to account for fluctuation-induced modifications of the classical dispersion relations, we also introduce running wave function renormalisations  $Z_q, Z_\phi$  and  $Z_\Delta$  for the quarks, the mesons and the diquarks respectively. The Pauli-Gürsey symmetry at vanishing chemical potential relates the meson and diquark Yukawa couplings to be  $h_\phi = h_\Delta = h$  as in (4). However, at finite  $\mu$  this symmetry is broken which

leads to manifestly different interactions of diquarks and mesons. To accurately account for this breaking we allow for different running Yukawa couplings  $h_\phi \neq h_\Delta$ . Higher order scale-dependent interactions between mesons and diquarks are taken into account by a scale-dependent effective potential  $V$ .

Taking all this into account, the quark sector of our truncation, i.e. the contribution to the effective action bilinear in the fermion fields, reads

$$\Gamma_q = \int_x Z_q \bar{q} \left( i \not{\partial} + i \sqrt{Z_\phi} h_\phi (\sigma + i \gamma_5 \vec{\tau} \cdot \vec{\pi}) + i \gamma_0 \mu \right) q + \int_x Z_q \sqrt{\frac{Z_\Delta}{2}} h_\Delta (i \Delta^* q^T C \gamma_5 \tau_2 t_2 q - \text{h.c.}) . \quad (16)$$

It contains the kinetic term for the quarks as well as the Yukawa interaction terms. The prefactor  $\sqrt{Z_\phi}$  in the Yukawa interaction is introduced in order to guarantee RG-invariance of the Yukawa couplings: the RG-scaling is carried by the factor  $Z_q \sqrt{Z_\phi}$ . Note however, that RG-invariance does not imply cutoff independence. The kinetic terms of the mesons and the diquarks are

$$\Gamma_\phi = \int_x \left\{ \frac{Z_\phi}{2} [(\partial_\mu \vec{\pi})^2 + (\partial_\mu \sigma)^2] - \sqrt{Z_\phi} c \sigma \right\} , \quad \Gamma_\Delta = \int_x Z_\Delta \left\{ (\partial_\tau - 2\mu) \Delta^* (\partial_\tau + 2\mu) \Delta + |\partial_i \Delta|^2 \right\} . \quad (17)$$

Note that we have included the explicit chiral symmetry breaking parameter  $c$  to the mesonic contribution. The derivative term of the diquarks includes the chemical potential and the factor  $\pm 2$  indicates the corresponding charge of the (anti-)diquark. We also have rescaled the diquark fields with a factor  $\sqrt{2}$  in comparison to (4), in order to obtain the conventional action of a complex scalar field. In our Euclidean setting the time axis is compactified on a torus with circumference  $\beta = 1/T$  at finite temperature. In case the  $SU(4)$  flavor symmetry is not violated, the relations  $Z_\phi = Z_\Delta$  and  $h_\phi = h_\Delta$  hold. In summary, the complete truncation of the full effective action reads,

$$\Gamma[\Phi] = \Gamma_q + \Gamma_\phi + \Gamma_\Delta + \int_x V(\vec{\varphi}) , \quad (18)$$

where  $\Phi = (\vec{\pi}, \sigma, \Delta, \Delta^*, q, \bar{q})$ , and the effective potential  $V(\vec{\varphi})$  contains the multi-meson diquark interactions. It is discussed in more detail in the next section.

## B. Effective Potential

At vanishing chemical potential two-flavor QC<sub>2</sub>D exhibits the  $SU(4) \simeq SO(6)$  Pauli-Gürsey flavor symmetry. At finite  $\mu$  this is broken to  $SO(4) \times SO(2)$ .  $SO(4)$  is related to the  $SU(2)_L \times SU(2)_R$  chiral symmetry and  $SO(2)$  is related to the  $U(1)_B$  baryon number symmetry. Hence,

the effective potential can be considered as a function of two invariants. Taking the explicit symmetry breaking into account, we have

$$U(\rho_\phi, \rho_\Delta, \sigma) = V(\rho_\phi, \rho_\Delta) - 4\mu^2 \rho_\Delta - c \sqrt{Z_\phi} \sigma , \quad (19)$$

where

$$\rho_\phi = \frac{Z_\phi}{2} (\vec{\pi}^2 + \sigma^2) , \quad \rho_\Delta = \frac{Z_\Delta}{2} (\Delta_1^2 + \Delta_2^2) , \quad (20)$$

are the invariants of the chiral and baryon number symmetry respectively. The field invariant  $\rho_\Delta$  is given in the real representation of the diquarks, which relate to the complex representation by  $\Delta = \frac{1}{\sqrt{2}}(\Delta_1 + i\Delta_2)$  and  $\Delta^* = \frac{1}{\sqrt{2}}(\Delta_1 - i\Delta_2)$ . The explicit current quark mass, which directly relates to the explicit symmetry breaking  $c$ , gives rise to a smooth chiral crossover. On the other hand, a rising chemical potential will lead to a second order phase transition to the BEC phase.

A non-vanishing vacuum expectation value  $\kappa_\phi$  of  $\rho_\phi$  signals chiral symmetry breaking and a non-vanishing vacuum expectation value  $\kappa_\Delta$  of  $\rho_\Delta$  signals the breaking of baryon number conservation. They are given by the stationary solution of the effective potential  $U$ :  $\partial_\phi U = \partial_\Delta U = 0$ . With (19) this leads to stationary conditions for the effective potential  $V$ . For the radial directions  $\sigma$  and  $\Delta_1$  these equations read

$$\left. \frac{\partial V}{\partial \rho_\phi} \right|_{\vec{\rho}=\vec{\kappa}} = \frac{c}{\sqrt{2\kappa_\phi}} , \quad \left. \frac{\partial V}{\partial \rho_\Delta} \right|_{\vec{\rho}=\vec{\kappa}} = 4\mu^2 . \quad (21)$$

where  $\vec{\rho} = (\rho_\phi, \rho_\Delta)$  and  $\vec{\kappa} = (\kappa_\phi, \kappa_\Delta)$ . The solution  $\kappa$  of (21) are the order parameters for the chiral and the BEC phase respectively.

## C. Flow of the Effective Potential

The flow of the effective potential  $U(\rho_\phi, \rho_\Delta)$  is that of the effective action, (5), depicted in Fig. 2, evaluated at constant bosonic fields and vanishing quarks. Then all quark terms and all derivative terms in the effective action vanish and the left hand side of the flow equation, (5), reduces to  $\partial_t U$ . With the flat 3d regulators specified in App. C, (C1), the spatial momentum integration is done readily. This leads to

$$\partial_t U(\rho_\phi, \rho_\Delta) = \frac{k^5 T}{6\pi^2} \sum_{n \in \mathbb{Z}} \left[ \left( 1 - \frac{\eta_\phi}{5} \right) [3G_\pi(k^2) + G_\sigma(k^2)] + 2 \left( 1 - \frac{\eta_\Delta}{5} \right) G_\Delta^+(k^2) + 4N_c N_f \left( 1 - \frac{\eta_q}{4} \right) A_+(k^2) \right] , \quad (22)$$

where the boson and fermion propagators  $G$  and  $A$  are given in App. B, and anomalous dimensions are defined as  $\eta_{\Phi_i} = -\partial_t Z_{\Phi_i} / Z_{\Phi_i}$ . The Matsubara summation can be

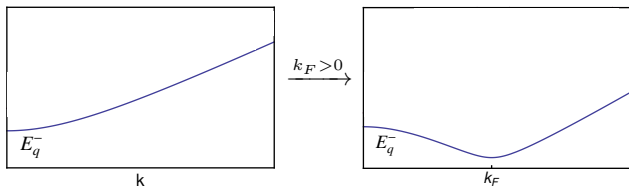


Figure 3: On the left-hand side we see the qualitative behaviour of the quark energy dispersion for the case  $k_F < 0$ . It is a monotonically rising functions with  $k$ . On the right-hand side we have the case  $k_F > 0$ . The dispersion develops a minimum at the Fermi surface, which indicates the formation of quark Cooper pairs.

carried out analytically, but due to the excessive length of the resulting equation we do not show it here.

The right hand side of the flow equation (22) depends on the energy dispersion relations of the fields, that can be read-off from the corresponding propagators in App. B. The onset of the diquark phase is reflected in these energy dispersion relations. In particular, the energy dispersion of the quarks is

$$E_q^\pm = \sqrt{(\epsilon_q \pm \mu)^2 + 2h_\Delta \rho_\Delta}, \quad \epsilon_q = \sqrt{k^2 + 2h_\phi \rho_\phi}. \quad (23)$$

At finite chemical potential a Fermi surface occurs and we define the corresponding Fermi energy as  $k_F^2 = \mu^2 - m_q^2$ , where  $m_q = \sqrt{2h_\phi \rho_\phi}$ . The quark energy dispersion  $E_q^-$  for the case  $k_F < 0$  in the phase with  $\rho_\Delta \neq 0$  is shown in the left plot of Fig. 3. The minimum of the energy dispersion at vanishing momentum  $k=0$  indicates that the diquark condensate is of the BEC type. When the chemical potential exceeds the quark mass, i.e.  $k_F > 0$ , the quark energy dispersion develops a minimum at non-vanishing momentum scale  $k_{\min} = k_F$ . This is shown in the right plot of Fig. 3. This is typical for a BCS-like ground state where the quarks form Cooper pairs. Hence,  $m_q = \mu$  can be used as an indication for the BEC-BCS crossover in the present case [20].

#### D. Flow of the Meson-Diquark Couplings

We expand the effective potential in the invariants  $\rho_\phi, \rho_\Delta$  about its flowing minimum  $\vec{\kappa}$ , see (21). For related recent FRG-applications on such a two-dimensional Taylor expansion for the effective potential see e.g. [62, 63]. Alternative evaluation methods of the flow of the effective potential are a grid of field values [33] or an expansion about a fixed background [45]. In such a two-dimensional Taylor expansion the potential reads

$$V(\rho_\phi, \rho_\Delta) = \sum_{\substack{n,m=0 \\ n+m < N}} \frac{\lambda_{n,m}}{n!m!} (\rho_\phi - \kappa_\phi)^n (\rho_\Delta - \kappa_\Delta)^m, \quad (24)$$

where the linear couplings are related to mass parameters,

$$\lambda_{1,0} = m_\phi^2, \quad \lambda_{0,1} = m_\Delta^2, \quad (25)$$

and  $\lambda_{0,0}$  determines the value of the potential  $V$  in the minimum,  $V(\vec{\kappa}) = \lambda_{0,0}$ . This is relevant for the thermodynamics of the system, as the pressure is related to  $V_T - V_{T=0}$ . In the present work we do not discuss the thermodynamical properties of QC<sub>2</sub>D, and drop the constant part.

Physically, the expansion in (24) constitutes an expansion of the effective potential in terms of multi-scattering processes of mesons and diquarks. By solving (21) with this parameterisation, we obtain the order parameters of chiral and baryon number symmetry breaking. For the chiral order parameter we find in all phases,

$$\kappa_\phi = \frac{1}{2} \left( \frac{c}{m_\phi^2} \right)^2, \quad (26)$$

For diquark condensation we distinguish two cases. The normal phase is defined by  $\kappa_\Delta = 0$ . The BEC regime is characterised by a non-vanishing diquark condensate  $\kappa_\Delta \neq 0$ . In this case (21) implies  $m_\Delta = 2\mu$ .

We have introduced an explicit symmetry breaking  $-c\sigma$  which is directly linked to non-vanishing current quark masses. Since the flow equation (5) is of second order in field derivatives, we infer from (19),

$$\frac{\partial}{\partial t} \left( c\sqrt{Z_\phi} \right) = 0 \quad \Leftrightarrow \quad \partial_t c = \frac{\eta_\phi}{2} c. \quad (27)$$

We want to emphasise that this term merely shifts the minimum of the effective potential without influencing the RG-flow of the effective potential itself. However, since we expand about this minimum,  $c$  enters the flow equations for the couplings via the expansion point.

The cutoff derivative of the effective potential at fixed  $\phi, \Delta$  in the parameterisation (24) hits  $\lambda_{n,m}$ , the flowing minimum  $\kappa$  as well as the renormalisation factors in  $\vec{\rho}$ . Therefore the  $\rho$ -derivatives of  $\partial_t U$  read

$$\begin{aligned} & \dot{\lambda}_{n,m} - \lambda_{n,m} (n\eta_\phi + m\eta_\Delta) - \lambda_{n+1,m} (\dot{\kappa}_\phi + \eta_\phi \kappa_\phi) \\ & - \lambda_{n,m+1} (\dot{\kappa}_\Delta + \eta_\Delta \kappa_\Delta - 4\mu^2 \delta_{n0} \delta_{m1}) \\ & = \frac{\partial^n}{\partial \rho_\phi^n} \frac{\partial^m}{\partial \rho_\Delta^m} \dot{U} \Big|_{\vec{\rho}=\vec{\kappa}}, \end{aligned} \quad (28)$$

where  $\dot{U}$  is given by the flow equation (22). The mesonic mass parameter  $m_\phi^2 = \lambda_{1,0}$  is connected to the expansion point  $\kappa_\phi$  via (26), and its flow is given by

$$\dot{m}_\phi^2 = -\frac{c}{(2\kappa_\phi)^{3/2}} (\dot{\kappa}_\phi - \eta_\phi \kappa_\phi). \quad (29)$$

Furthermore, the cutoff-dependence of the diquark condensate and mass parameter in the different phases can

be inferred from (21) and we find

$$\begin{aligned} \text{Normal regime:} \quad & \kappa_\Delta = \kappa_\Delta = 0, \\ \text{BEC regime:} \quad & \dot{m}_\Delta^2 = 0, \quad m_\Delta^2 = (2\mu)^2. \end{aligned} \quad (30)$$

Finally, we discuss the implications of the Silver Blaze property (7): the couplings  $\lambda_{n,m}$  carry baryon number  $2m$ . Hence, at vanishing temperature and below the onset chemical potential  $\mu_c$  they are functions of  $\tilde{p}_i$ , see (7). Accordingly, Silver blaze is violated with an expansion at  $p = 0$  as is done for the flow of the effective potential. Indeed it relates to a  $\mu$ -dependent expansion point  $\tilde{p} = i\mu$ . We emphasise that this has nothing to do with the Taylor expansion used here, but Silver blaze breaking is introduced by considering constant diquark fields, leading to (22). Indeed, in contradistinction to a grid solution of (22) the present Taylor expansion gives us the possibility to even cure the mild Silver blaze breaking. First, we can evaluate the flow of the couplings  $\lambda_{n,m}$  at  $\tilde{p}_i = 0$ . This possibility will be explored in a subsequent work. Second, we may enforce the Pauli-Gürsey symmetry also in the presence of a non-vanishing chemical potential and only expand the effective potential in the meson field. This possibility is explored in the App. D and neglects the physics effects of the breaking of the Pauli-Gürsey symmetry. Given the good convergence of the derivative expansion this is less trustworthy.

In summary, the derivative expansion at vanishing momenta  $p_i = 0$  employed in this work is based on the assumption of a mild  $\tilde{p}$ -dependence. Hence we expect the breaking of Silver blaze to be minimal, and we shall prove below that this is indeed the case.

### E. Anomalous Dimensions

The cutoff-dependent wave function renormalisations enter the flow equations through the corresponding anomalous dimensions  $\eta_\Phi = -\partial_t Z_\Phi / Z_\Phi$ . In the spirit of the derivative expansion used here we evaluate them at vanishing momentum. For the bosonic anomalous dimensions this entails that the evaluation point is at  $p^2 = 0$ . Following our discussion in Sec. II C this results in a manifestly  $\mu$ -dependent bosonic wave function renormalisations below  $\mu_c$ . However, we demonstrate in App. A 3 that the resulting violation of the Silver Blaze property is minor. In summary, we define the bosonic anomalous dimensions via

$$\eta_{\varphi_i} = -\frac{1}{Z_{\varphi_i}} \frac{\partial}{\partial \tilde{p}^2} \dot{\Gamma}_{\varphi_i \varphi_i} \Big|_{p=0}, \quad (31)$$

where we use  $\varphi_1 = \pi_1$  for the mesons and  $\varphi_6 = \Delta_2$  for the diquarks. For explicit flow equations see App. C.

Now we turn to the fermionic anomalous dimension, which we define via

$$\eta_q = -\frac{1}{3N_f N_c Z_q} \text{Re} \left[ \frac{\partial}{\partial \tilde{p}} \cdot \text{tr} \left( \tilde{\gamma} \dot{\Gamma}_{\bar{\Psi} \Psi} \right) \Big|_{p=p_{\min}} \right]. \quad (32)$$

$\Psi$  represents the fermions in Nambu-Gorkov formalism defined in App. B 2. The trace acts in all fermionic subspaces, i.e. color-space, spinor-space and flavor space. The explicit flow equation is shown in App. C. Since fermions do not have a vanishing Matsubara mode, we define the quark anomalous dimension at the minimal momentum  $p_{\min} = (\pi T, \vec{0})$  at finite temperature [45]. This procedure guarantees that fermion and boson propagators always carry the correct Matsubara frequency in the loops. However, as a result,  $Z_q$  is a function of  $(\pi T - i\mu)$  which, in addition to the explicit  $\mu$ -dependence, renders the anomalous dimension complex valued. In order to keep the effective action real, we project out the real part in (32). As for the bosonic wave function renormalisations, we demonstrate in App. A 3 that the violation of the Silver Blaze property which results from the present momentum-independent approximation of  $Z_q$  is very small.

### F. Flow of the Yukawa Couplings

We can extract the running of the meson and diquark Yukawa coupling from the flow of the quark two-point function similarly to [45] and find

$$\begin{aligned} \partial_t h_\phi &= \left( \eta_q + \frac{\eta_\phi}{2} \right) h_\phi - \frac{1}{4N_f N_c} \text{Re} \left[ \text{tr} \frac{i \dot{\Gamma}_{\bar{\Psi} \Psi}}{Z_q Z_\phi^{1/2} \sigma} \right], \\ \partial_t h_\Delta &= \left( \eta_q + \frac{\eta_\Delta}{2} \right) h_\Delta + \frac{1}{4N_f N_c} \text{Re} \left[ \text{tr} \hat{P} \frac{\dot{\Gamma}_{\bar{\Psi} \Psi}}{Z_q Z_\Delta^{1/2} \Delta} \right]. \end{aligned} \quad (33)$$

Here,  $\hat{P}$  is the projection matrix on the diquark term in the inverse quark propagator, see App. B, (B24). Eq. (33) provide flows for field and momentum-dependent couplings. In the present work we evaluate the flows on the flowing minimum  $\vec{k}$  as well as vanishing momentum. The explicit expressions for the resulting flow equations are deferred to App. B. The flow of both couplings is complex at finite temperatures similarly as that of the anomalous dimensions discussed in the previous section. Our projection (33) is chosen such, that this does not lead to a complex action. Moreover, the Silver Blaze violation related to the expansion at vanishing momentum is small, see App. A 3.

### G. Initial Conditions

In Tab. I the initial conditions are displayed for different truncations. The full truncation used in the present work is denoted as 2d Taylor'. It has three running wave function renormalisations  $Z_\phi$ ,  $Z_\Delta$ ,  $Z_q$ , and two running Yukawa couplings  $h_\phi$ ,  $h_\Delta$ . The Taylor expansion is done up to the order  $N = 5$  in the  $\rho$ 's. In the UV we start with an  $SO(6)$  symmetric potential.

	$\Lambda$ [MeV]	$\langle\sigma\rangle_\Lambda$ [MeV]	$m_{\phi,\Lambda}$ [MeV]	$\lambda_{2,0,\Lambda}$	$h_{\phi,\Lambda}$	$m_\pi$ [MeV]	$2\mu_c$ [MeV]
2d Taylor'	900	2.28	1135	89.0	6.43	143	138
2d Taylor	900	4.50	650	7.0	4.80	158	139
2d Taylor [33]	900	39.94	247	76.3	4.80	180	143
$f_\pi = 93$ MeV	900	7.55	566	45.8	4.14	138	132

Table I: Initial conditions for the UV action  $\Gamma_{k=\Lambda}$ , resulting pion masses  $m_\pi$  in the vacuum and the corresponding critical chemical potential for the onset of diquark condensation at  $T = 0$ . The prime denotes that running Yukawa couplings and wave function renormalisations are included. In the third row are the initial conditions used in [33], where an LPA was solved on a 2d grid. The resulting  $m_\pi$  and  $2\mu_c$  are shown for our 2d Taylor method, and are close to what was found in [33].

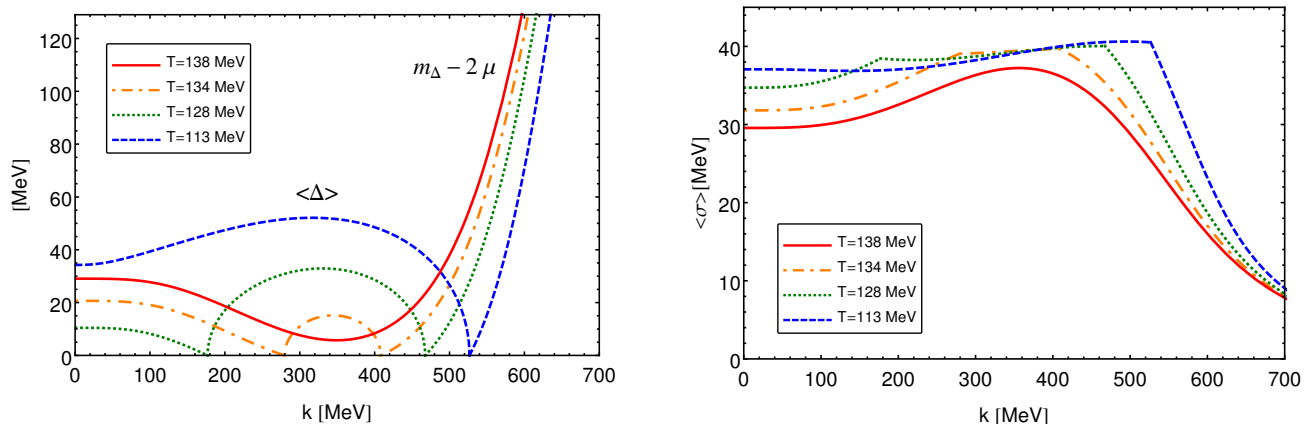


Figure 4: Flow of the diquark mass and condensate  $\langle\Delta\rangle = \sqrt{2\kappa_\Delta}$  (left panel), as well as the chiral condensate  $\langle\sigma\rangle = \sqrt{2\kappa_\phi}$  (right panel) for  $\mu = 100$  MeV and different temperatures within the 2d Taylor' truncation. The critical temperature for this choice of  $\mu$  is  $T_c \approx 125$  MeV. We see that the system exhibits finite domains of non-vanishing diquark condensate close to the transition to the BEC phase.

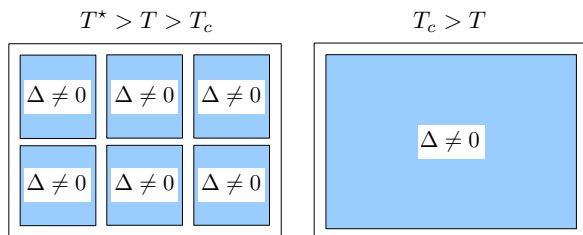


Figure 5: Illustration of the pre-condensation effect. At temperatures close to  $T_c$  local domains of condensation form (left figure). Below  $T_c$  the whole volume is filled with a condensate (right figure).  $T^*$  is the temperature where pre-condensation sets in. It marks the outer edge of the shaded blue area in the right plot of Fig. 6.

The initial conditions for the first two cases in the table are tuned such that we obtain an  $\sqrt{N_c}$ -scaled pion decay constant of  $f_\pi = \langle\sigma\rangle|_{k=0} = 76$  MeV in the vacuum instead of the usual  $f_\pi \approx 93$  MeV. Further conditions are that the vacuum quark mass comes in  $m_q \approx 360$  MeV in the IR, and that the onset of the diquark condensation should be at  $2\mu_c \approx 138$  MeV.

Note that physically sensible initial conditions in the chirally symmetric phase feature small coupling strengths

and large masses of the bound states, which reflect their nature as auxiliary fields in this phase. Hence, in addition to the initial conditions for the LPA taken from [33], we have chosen the set shown in the second row of Tab. I. We see that this choice already reduces the difference between curvature mass of the pion and onset chemical potential by about 50% as compared to the initial values taken from the reference.

For completeness, we also show initial conditions which yield  $f_\pi \approx 93$  MeV and  $m_q \approx 340$  MeV in the vacuum in the fourth row of Tab. I. The main results of this work are obtained with the 2d Taylor' initial conditions.

## IV. RESULTS

### A. Pre-condensation

The RG flows of the order parameters of our model close to the BEC transition exhibit a peculiar behaviour known as pre-condensation. In Fig. 4 we show the flows of the diquark mass and condensate as well as the chiral condensate at  $\mu = 100$  MeV for various temperatures in the vicinity of the BEC transition. We observe that at temperatures slightly above  $T_c$  the flowing diquark mass

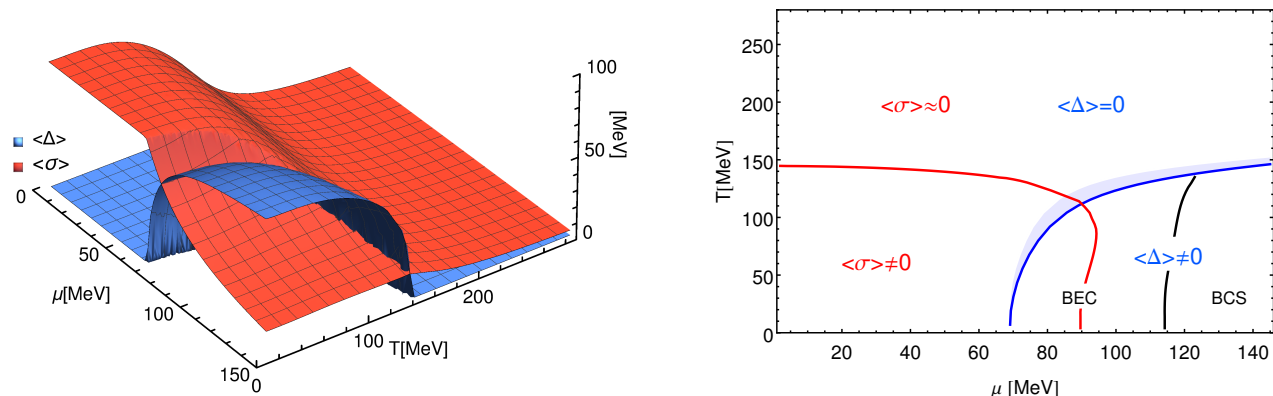


Figure 6: The phase diagram of QC<sub>2</sub>D in the 2d Taylor' truncation. Right panel: The red line marks the chiral phase boundary which is defined by the maximum of the chiral susceptibility, see Ref. [45]. The blue line is the boundary of the diquark/superfluid phase defined by  $\lim_{k \rightarrow 0}(m_\Delta - \mu_\Delta) = 0$ . The blue shaded area marks the pre-condensation phase. The black line of the BEC-BCS crossover is where  $h_\psi(\sigma) = \mu$ .

vanishes at an intermediate scale. Below this scale a non-vanishing diquark condensate appears and vanishes again before all fluctuations are integrated out towards  $k = 0$ , i.e., the system ends up in the chirally symmetric phase, see the left panel Fig. 4. We refer to this behaviour as pre-condensation. This phenomenon is an analogue to the one known from the ferromagnetic transition close to the Curie temperature. It has also been observed within FRG-applications, e.g., in ultra cold atoms [51]. Here, we show for the first time that pre-condensation is also a phenomenon in QC<sub>2</sub>D. The occurrence of a diquark condensate at intermediate scales means that small domains of non-vanishing diquark condensates develop which eventually average out upon considering larger volumes, see Fig. 5. The left panel of Fig. 4 shows that the regime of intermediate diquark condensation grows with decreasing temperature. Hence, these domains become larger until a single domain fills the entire volume below the critical temperature, cf Fig. 5.

Pre-condensation also manifests itself in the chiral condensate. The corresponding flow is shown in the right panel of Fig. 4. The finite range of scales where intermediate diquark condensation occurs, gives rise to a plateau in the chiral condensate in the same range. This can be related to a qualitative change in the bosonic contributions to the flow of the chiral condensate in the presence of an intermediate diquark condensate and the concomitant Goldstone fluctuations.

## B. The QC<sub>2</sub>D Phase Diagram

The phase diagram of two-color QCD within our full truncation is presented in Fig. 6, showing the chiral phase transition and the occurrence of the diquark condensate

as a function of chemical potential and temperature. At small chemical potential and small temperatures the pronounced quark fluctuations drive chiral symmetry breaking leading to a non-vanishing chiral condensate. Here, an increase of the temperature causes a suppression of quark fluctuations and therefore induces a smooth crossover to the chirally symmetric regime. Bosonic fluctuations additionally contribute to a flattening of the crossover.

At vanishing temperature, we obtain the onset of diquark condensation at a chemical potential of  $\mu = m_\pi/2$  via a second order phase transition. For diquark chemical potentials  $\mu_\Delta = 2\mu$  exceeding their excitation gap or mass, the system is populated with diquarks, forming the condensate at small temperatures. The diquark condensate triggers a decay of the chiral condensate because the condensation of quarks into quark-quark states is preferred over quark-antiquark pairing. Due to the small mass of the baryonic bound states, the chiral condensate starts decaying smoothly at much smaller chemical potentials as compared to QCD and there is no trace of a critical endpoint. Furthermore, a BCS pairing of quarks with opposite momenta on the Fermi surface occurs when the chemical potential exceeds the quark mass, cf. Sec. III C.

In the left panel of Fig. 7, we explicitly compare the results for the condensates at temperature  $T = 0$  obtained in various works, namely lattice calculations [23], the NJL model [13], the tree-level linear sigma model [16], different FRG approaches [33] and this work. All methods agree qualitatively, however, at larger chemical potential sizeable quantitative corrections can be observed. For the different FRG approaches, these differences can be related to the additional fluctuation effects induced by the running wave function renormalisations and the running Yukawa couplings which have been omitted in the LPA calculation in [33]. We further note that the diquark

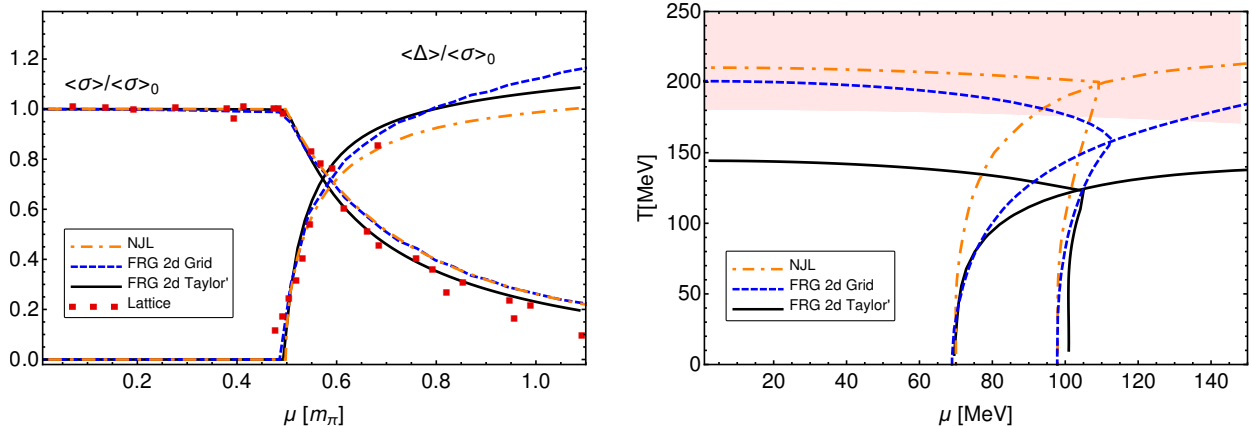


Figure 7: Meson and baryon condensates at vanishing temperature (left panel) as well as the phase diagram (right panel) for various truncations and methods. The “FRG 2d Grid” results are taken from [33] and the NJL results from [13]. The lattice data is from [23]. Chiral phase boundaries are computed via the half value of the order parameters and the red shaded area indicates the region where the effective models become invalid.

condensate obtained from the purely fermionic NJL model agrees well with the lattice results where bosons are heavy.

In the right panel of Fig. 7, we compare the corresponding finite temperature phase diagrams showing results from the NJL model and the various FRG approaches. Here, the chiral crossover is defined by the half value of the order parameter. The considerable quantitative effects within the FRG approach, induced by taking into account the running of Yukawa couplings and wave function renormalisations are clearly exposed by comparing 2d Taylor’ and 2d Taylor results for the critical temperature at vanishing density. While we find  $T_c \approx 150$  MeV for 2d Taylor’, see Fig. 7, we have  $T_c \approx 210$  MeV, see Fig. 14 for the 2d Taylor approximation with the same initial condition. Indeed the latter critical temperature is found for all LPA approximations with different initial conditions, see Fig. 14. This underlines the quantitative importance of the wave function renormalisation and the Yukawa coupling. Hence, non-classical dispersion relations as well as quantum corrections to the quark-boson interactions play a crucial role for an accurate description of the phase structure of QC<sub>2</sub>D. To corroborate this statement, we demonstrate in App. A 2 that this large effect cannot be ascribed to different initial conditions.

The NJL result has the highest critical temperatures for both, the chiral crossover and the superfluid phase transitions. In the FRG computation within the LPA the phase boundaries are lowered by about 10% through the inclusion of symmetry-restoring bosonic fluctuations. The additional effects considered in the present work lead to a further decrease of the phase boundary of about 30%, cf. Fig. 7, see App. A 2 for details. At high temperatures, the cutoff scale  $\Lambda$  constrains the applicability of the effective low-energy description presented here, as indicated by the red-shaded area in Fig. 7. Here, the initial conditions become effectively temperature and density dependent, see App. A 4 for details.

### C. Mass Spectrum

Now, we discuss the curvature masses of mesons and diquarks for the normal as well as for the BEC phase in the meson sector

$$\begin{aligned} \text{normal:} \quad m_\pi &= m_\phi, \quad m_\sigma = \sqrt{m_\phi^2 + 2\kappa_\phi \lambda_{2,0}}, \\ \text{BEC:} \quad m_\pi &= m_\phi, \quad m_{\bar{\sigma}} = \sqrt{m_1^2 - m_2^2}, \end{aligned} \quad (34)$$

and in the baryon sector

$$\begin{aligned} \text{normal:} \quad m_{\Delta,+} &= m_\Delta + 2\mu, \quad m_{\Delta,-} = m_\Delta - 2\mu, \\ \text{BEC:} \quad m_{\bar{\Delta}_1} &= \sqrt{m_1^2 + m_2^2}, \quad m_{\Delta_2} = 0. \end{aligned} \quad (35)$$

Here, we have defined the mass parameters

$$\begin{aligned} m_1^2 &= \frac{m_\sigma^2}{2} + 8\mu^2 + \kappa_\Delta \lambda_{0,2}, \\ m_2^2 &= \sqrt{m_1^4 - 2\kappa_\Delta (m_\sigma^2 \lambda_{0,2} - 2\kappa_\phi \lambda_{1,1}^2) - 16m_\sigma^2 \mu^2}, \end{aligned}$$

and  $m_\sigma$  is the expression for the sigma mass in the normal phase. The sigma state and one of the diquark states are mixtures of the original states. Further,  $\Delta_2$  is the Goldstone mode associated with the breaking of  $U(1)_B$ .

In Fig. 8, we present the temperature and chemical potential dependence of the masses. At vanishing chemical potential, see left panel of Fig. 8, the pion and the diquark masses are degenerate. For large temperatures, where chiral symmetry is restored, they join with the sigma mass and all bound states decouple from the system. For vanishing temperature, see right panel of Fig. 8, the diquark starts condensing at  $\mu_c = \frac{m_\pi}{2}$  and the behaviour of the masses changes accordingly. At large chemical potential chiral symmetry is restored and  $m_{\bar{\sigma}} \rightarrow m_\phi$ . Then,

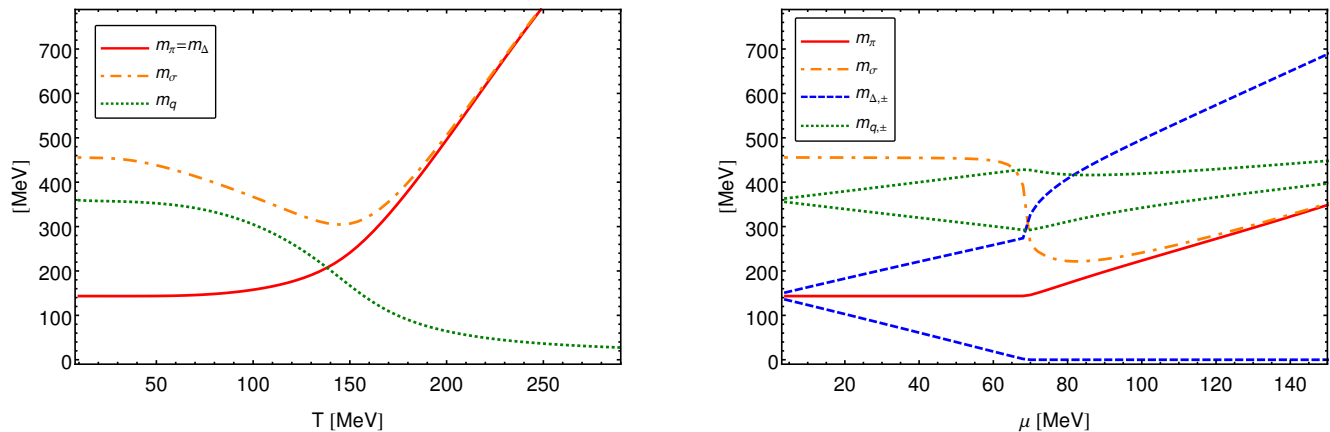


Figure 8: Mass spectrum of two-color QCD within the 2d Taylor' truncation. The chiral crossover and the phase transition to the BEC phase are clearly visible from the behaviour of the masses. In the left panel ( $\mu \approx 0$ ) the quark mass goes from being small to being large with decreasing temperature, while the pions and diquarks become the pseudo-Goldstone modes splitting up from the sigma. In the right panel ( $T \approx 0$ ) we have a phase transition at  $\mu = \frac{m_\pi}{2}$ . Even though chiral symmetry is restored at asymptotic  $\mu$ , the quarks do not become massless because they are coupled to the diquark condensate.

the sigma and the pions are degenerate. Accordingly, the corresponding (anti-)quark masses are given by the relation

$$m_{q,\pm} = \sqrt{(\hat{\sigma} \pm \mu)^2 + \hat{\Delta}^2}, \quad (36)$$

and again chiral symmetry is restored at large  $\mu$ .

## V. CONCLUSIONS

In this work, we add important aspects to the understanding of the high density regime of QCD by investigating a modification of QCD with two colors. The absence of a fermion sign problem in this model has drawn the interest of the lattice community for over a decade now. Here, we refine an alternative non-perturbative approach based on the functional renormalisation group.

More specifically, we employ an effective low-energy model for  $QC_2D$  where the gluon degrees of freedom have been integrated out. This amounts for a description of the theory in terms of quarks, mesons and diquarks. The diquarks are color neutral objects and constitute the baryons of the theory. Therefore, we have a playground at hand to study baryonic degrees of freedom in a simplified bosonic description as well as a relativistic BEC-BCS crossover. The FRG-approach allows to interpolate between the microscopic and the macroscopic regime of the theory, by integrating out all thermal and quantum fluctuations. It generates all correlations that are allowed by the underlying symmetries. By examining the flow equation of the effective potential, we study the interplay of bosonic and fermionic degrees of freedom for different temperatures and chemical potential. The chiral condensate goes through a crossover towards large temperatures, where chiral symmetry is restored. The diquark condensate sets in via a second order phase transition at large

chemical potential and small temperatures.

For the first time in the context of two-color QCD, we trace the momentum scale dependence of the diquark condensate and exhibit the phenomenon of pre-condensation: Small domains of non-vanishing diquark condensates appear at intermediate RG scales, however, no finite condensate persists as all fluctuations are integrated out. Therefore, the pre-condensation phase is a precursor of the BEC phase. Further, we find that the phase boundaries in our full truncation are significantly corrected upon inclusion of dynamical quark-hadron interactions and non-classical dispersions. We conclude that an inclusion of these effects is an important ingredient for a reliable determination of the phase boundaries in the phase diagram of  $QC_2D$ . Most strikingly, the chiral phase transition does not have a critical endpoint in the presence of diquark fluctuations.

Eventually, as an essential aspect of this work, we thoroughly studied the Silver Blaze property in the FRG framework. We exhibited that at vanishing temperature it amounts to a shift of the frequencies by the chemical potential with the appropriate charges. In case this property holds true at the initial scale, it is preserved by the flow equation, owing to its one-loop structure. However, this requires a full momentum resolution of all quantities, which are directly sensitive to the chemical potential. The diquark sector is strongly affected by this complication, if its parameters are not identified with the meson sector. Importantly, running wave function renormalisations considerably reduce the discrepancy between the onset chemical potential and the pion mass in the two-color case.

A natural next step of our work is to incorporate a phenomenological Polyakov-loop potential to investigate confinement in two-color QCD, cf. [44] for a LPA study. Further, a dynamical connection of the quark-gluon regime with the low-energy effective regime should be established, cf. Refs. [55, 56, 64].

*Acknowledgments* - We thank Nils Strodthoff, B.-J. Schaefer and L. von Smekal for discussions. This work is supported by the Helmholtz Alliance HA216/EMMI, the grant ERC-AdG-290623, the FWF grant P24780-N27, and the BMBF grant 05P15VHFC1.

## Appendix A: Truncation Effects

In this section we study to some extent the reliability of our truncation by analysing the violation of Silver-Blaze, the convergence of our expansion, the effects of different parts of our truncation and in-medium cutoff effects.

### 1. Silver-Blaze Violation

In Fig. 9 we show the flows of the relevant and marginal hadronic couplings for  $T=0$  at two choices of the chemical potential,  $\mu=0$  (vacuum) and  $\mu=0.4 m_\pi$ . Due to the  $SO(6)$  symmetry between meson and diquarks in the vacuum, all coefficients  $\lambda_{n,m}$  of a given order  $N$  with  $n+m=N$  are identical. They are represented by the solid red lines in Fig. 9. According to the Silver Blaze property, all  $n$ -point functions have to be independent of the chemical potential at vanishing temperature and for  $\mu < \mu_c$ . This implies that all couplings  $\lambda_{n,m}$  of a given

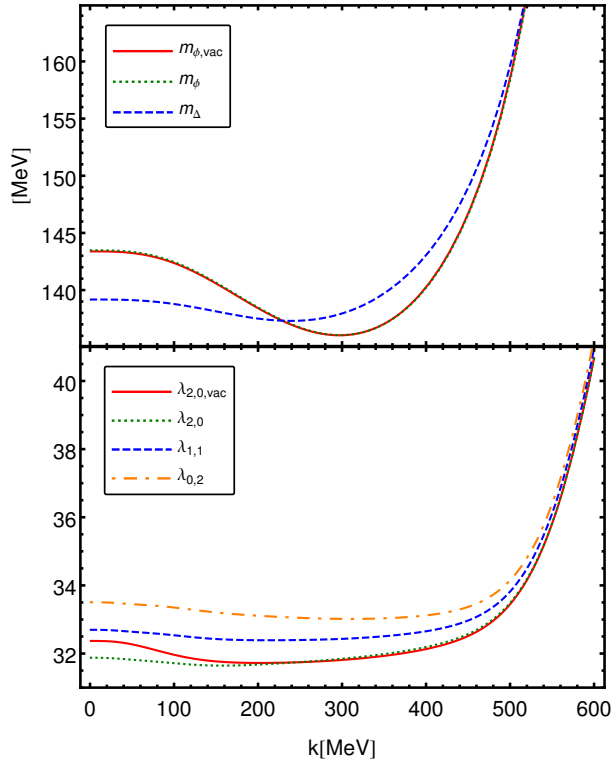


Figure 9: Flow of the mass parameters and four-point couplings. The red lines represent the vacuum flow, i.e. at  $T=\mu=0$ , the other lines are at  $\mu=0.4 m_\pi$ .

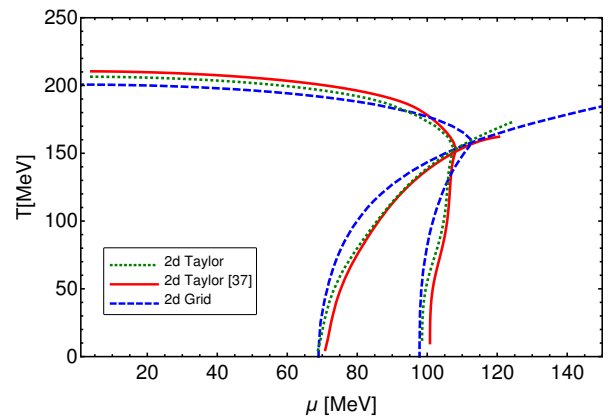


Figure 10: The phase boundaries from the grid method [33] and the Taylor method with different initial conditions. The initial conditions of “2d Taylor [37]” are the same as in the reference. Hence, A comparison between solid red line and the dashed blue line can be used to estimate how well the Taylor expansion is converged. The initial conditions of “2d Taylor” feature comparably weakly interacting heavy mesons at the initial scale. A comparison between the dotted green line and the solid red line can therefore be used to estimate the effect of different initial conditions on the phase boundaries. The initial conditions are given in Tab. I and are discussed in Sec. III G.

order  $N$  with  $n+m=N$  also have to be identical in this regime, i.e. also for  $\mu=0.4 m_\pi$ . The deviations of this expectation, see Fig. 9, therefore show the extent of the violation of the Silver Blaze property. The higher the order of the diquark fields (i.e. the second index) the sooner the flow starts to separate from the vacuum flow. This also couples back to the purely mesonic couplings. It is interesting that  $\lambda_{2,0}$  starts to deviate from the vacuum flow at around  $k \approx 2\mu$ . Nevertheless, even though higher order terms have a large deviation, they do not couple back very strongly to the physically important quantities:  $m_\Delta = \sqrt{\lambda_{0,1}}$  has only a deviation of about 5 MeV.

Following our discussions in Sec. II C and III C, this violation is well understood. Owing to our momentum independent expansion scheme, we generate explicitly  $\mu$ -dependent couplings. Then the chemical potential enters the flow of the effective potential through curvature contributions in diquark direction. Therefore, the higher the order of the diquark fields in a given  $n$ -point function, the larger the violation of Silver Blaze. However, our results presented in the previous section show only a minor violation implying that the back-coupling of the violation in the  $n$ -point functions to the physical observables is small.

### 2. Convergence of the Expansion

Here we study the convergence of our Taylor expansion. To measure its quantitative error we compare the results in the LPA to the results obtained on a two-dimensional

grid with the same truncation in [33]. This is shown in Fig. 10. The deviation between the two-dimensional Taylor expansion (solid red line) and the grid solution (dashed blue line) can be traced back to the lack of convergence in the LPA part of our truncation, cf. also App. D. However, we have shown in Sec. IV B and in particular the right panel of Fig. 7 that the error of neglecting effects beyond LPA is about 30%. Hence, regarding the systematic quantitative improvements within the present work, the error related to the expansion of the effective potential is only minor. We will discuss the effects that go beyond the LPA in the next section.

Interestingly, we also see in Fig. 10 that there is only a small difference between the phase boundaries obtained with the initial conditions shown in the second and third row of Tab. I, named “2d Taylor” (dotted green line) and “2d Taylor [37]” (solid red line) respectively. We note that the initial conditions “2d Taylor” are chosen in the same spirit as the initial conditions for our full truncation: As appropriate for the chirally symmetric phase, the bosonic interactions are weak and bosons are heavy and therefore decoupled from the system. Hence, as discussed in Sec. IV B, the large difference between the phase diagram from the LPA in [33] and from our full truncation in Fig 7 can be attributed to the highly relevant fluctuation effects that induce the running of the Yukawa couplings and the wave function renormalisations.

### 3. Truncation Effects Beyond the LPA

Here, we will investigate the truncation effects beyond the LPA. In the present case, we study the effect of a running meson and diquark Yukawa couplings and running quark and hadron wave function renormalisations. In Fig. 11 we show the chiral condensate as well as the critical temperature for different subsets of our full truncation (18). Here, “LPA” has the running effective potential as well as the running quark, meson and diquark wave function renormalisations, but a constant bare Yukawa coupling. Note that the renormalised Yukawa couplings have a trivial running induced by the non-vanishing anomalous dimensions. On the other hand, “LPA+h” takes the running of the effective potential and the Yukawa couplings into account, but has vanishing anomalous dimensions.

We see large effects on both, the chiral order parameter and the critical temperature. In general, we conclude that for fixed initial conditions and compared to LPA, the Yukawa coupling increases the critical temperature, while the running wave function renormalisations decrease it. The former effect is due to increased quark fluctuations which, in turn, lead to a larger phase of broken chiral symmetry. The latter is a result of the large positive bosonic anomalous dimensions in the vicinity of the phase transition, see e.g. Fig. 12. Since the initial masses in the UV are fixed for all truncations, the meson masses in LPA’ are driven to smaller values by the increasing wave function

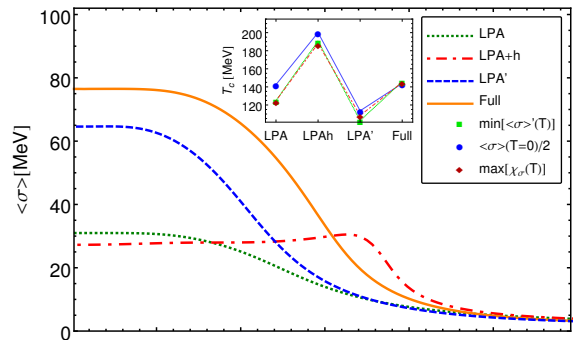


Figure 11: The chiral condensate as a function of temperature and the transition temperatures at  $\mu = 0$  for different truncations. The Taylor expansion is to the order  $N = 5$ .

renormalisations towards the IR as compared to LPA. Hence, bosonic fluctuations lead to a larger symmetric phase in the  $T-\mu$  plane. This has also been observed in a quark-meson model for low-energy QCD in [45]. At fixed initial conditions the effects of running Yukawa couplings and wave function renormalisations almost cancel for the critical temperature. This is in contrast to the case where for each truncation the initial conditions were tuned to the phenomenological IR parameters as it is shown in the right panel of Fig. 7. There, we see that the critical temperatures of LPA and our full truncation differ by about 30%.

Finally, we want to take a closer look at the in-medium modifications of the wave function renormalisations and the Yukawa couplings. In Fig. 12 the temperature/chemical potential dependence of the wave function renormalisations and the Yukawa couplings is shown. We see that the bosonic wave function renormalisations indicate in which regime the mesons/diquarks become auxiliary fields. Decreasing bosonic wave function renormalisations, e.g. towards large temperatures, imply that the corresponding fields become auxiliary [55, 64]. The left figure shows that, while the quark wave function renormalisation does not change much, the meson and diquark wave function renormalisations decrease in the vicinity of the critical scale with increasing temperature and at vanishing density. This implies a suppression/decoupling of bosonic fluctuations in the chirally symmetric phase.

The right plot shows the behaviour of the wave function renormalisations as a function of the chemical potential at vanishing temperature. Upon entering the BEC-phase, diquark fluctuations are enhanced, while meson fluctuations decouple.

Furthermore, despite the momentum-independent approximation we employ in this work, we see only a very weak dependence on the chemical potential below  $\mu_c = m_\pi/2$  of the quantities shown in the right plot of Fig. 12. The largest violation of the Silver Blaze property is visible in the diquark wave function renormalisation. This is not surprising since this is a purely baryonic quantity. In general, the mild dependence on  $\mu$  below  $\mu_c$  hints

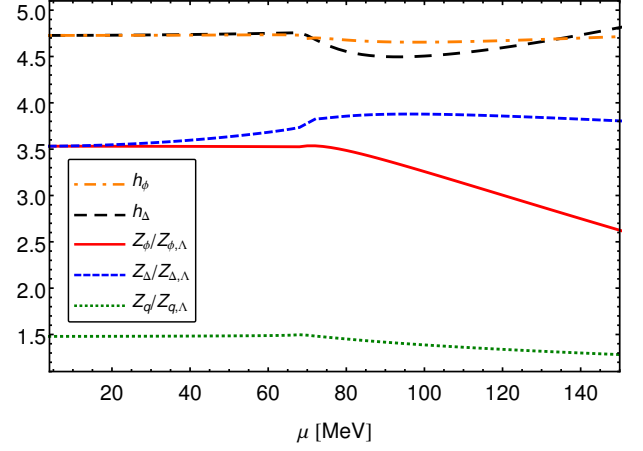
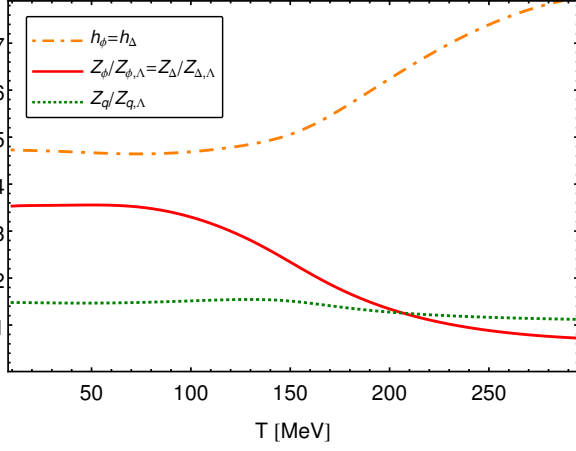


Figure 12: The Yukawa couplings and the wave function renormalisations as functions of  $T$  at  $\mu=0$  (left) as well as functions of  $\mu$  at  $T=0$  (right). The wave function renormalisations are normalised to their initial values in the UV. The explanations of each parameter can be found in the respective paragraphs.

at a rather mild frequency dependence of these quantities. This justifies the use of the lowest order derivative expansion in the present work a posteriori.

#### 4. In-Medium Cutoff Effects

In Fig. 13 we show the cutoff dependence of the chiral order parameter. For this study we used the initial conditions in the second row of Tab. I and solved the flow equations down (or up) to each of the  $\Lambda$ 's shown in the figure in the vacuum. Note that we tuned our initial conditions at  $\Lambda=900$  MeV. Then each time we used this as the starting point for the finite temperature calculations. However, we always started with a quartic potential in the UV, meaning that the higher order coupling are set to zero at every  $\Lambda$ . This is why we see small deviations at  $T=0$ , which can be regarded as a subsidiary probe for the convergence of the Taylor expansion. In any case, we clearly see rising deviations at large temperatures with the lowering of the cutoff. If the microscopic action feels the in-medium effects, it is not really microscopic. In this regime, the scale of thermal fluctuations exceeds the initial scale. In particular the crossover temperature should be independent of the cutoff. In the inset we observe that for cutoffs  $\Lambda > 800$  MeV it starts to converge.

The red shaded area in Fig. 7 marks the region where

$$\left| \frac{\dot{\Gamma}_{\Lambda, T, \mu} - \dot{\Gamma}_{\Lambda, 0, 0}}{\dot{\Gamma}_{\Lambda, 0, 0}} \right| > 0.1. \quad (\text{A1})$$

This measures the difference between the initial flow of the effective action in the medium and in the vacuum. If this quantity is large, it means that the microscopic action is considerably influenced by in-medium effects. In order to guarantee cutoff-independence of our results, the UV-cutoff has to be chosen large, i.e.  $\Lambda \gtrsim 800$  MeV. On

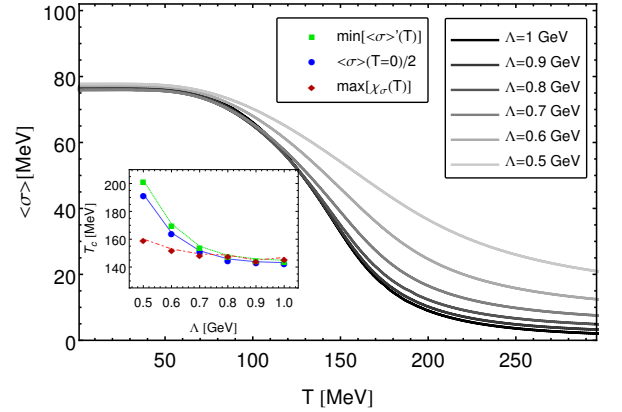


Figure 13: Chiral condensate and transition temperatures at  $\mu=0$  for different cutoff scales  $\Lambda$ .

the other hand, the initial scale should not be larger than the scale of validity of the model. For our effective low energy models we must remain below the scale where gluon degrees of freedom are relevant. Thus,  $\Lambda$  is constrained from both sides.

#### Appendix B: Propagators and Vertices

The propagator is defined by taking two functional derivatives of the effective action (18) with respect to the fields, adding the regulator and then evaluating at the expansion point, before taking the inverse. We employ a 3d flat regulator. Hence, only the space-like momenta are

regularised,  $\vec{p} \rightarrow \vec{p}_r$ , with

$$\vec{p}_r = \begin{cases} \vec{p} \sqrt{1 + r_B(\vec{p}^2/k^2)} & \text{for bosons,} \\ \vec{p}(1 + r_F(\vec{p}^2/k^2)) & \text{for fermions.} \end{cases} \quad (\text{B1})$$

Therefore we will omit the regulator terms in this section, while for the flow equations the momenta can simply be replaced by the regularised ones. The time-like components of the momenta are replaced by the Matsubara frequencies  $\omega_n = 2n\pi T$  for bosons and  $\nu_n = (2n + 1)\pi T$  for fermions.

### 1. Bosons

Here we will explicitly display the boson propagator for the real representation  $\varphi = (\vec{\pi}, \sigma, \Delta_1, \Delta_2)$  as well as the complex representation  $\bar{\varphi} = (\vec{\pi}, \sigma, \Delta, \Delta^*)$ . The relation is given by  $\Delta = (\Delta_1 + i\Delta_2)/2$ . The expansion points are given by  $\varphi_0 = (\vec{0}, \sqrt{2\rho_\phi/Z_\phi}, \sqrt{2\rho_\Delta/Z_\Delta}, 0)$  and  $\bar{\varphi}_0 = (\vec{0}, \sqrt{2\rho_\phi/Z_\phi}, \sqrt{\rho_\Delta/Z_\Delta}, \sqrt{\rho_\Delta/Z_\Delta})$ , where we leave the  $\rho$ 's as variables. The flow equation preserves the symmetries of the action, hence we can always rotate any other choice of  $\varphi_0$  and  $\bar{\varphi}_0$  with the corresponding symmetry group, which, at finite chemical potential, is  $O(4) \times O(2)$  for the real representation and  $O(4) \times U(1)$  for the complex representation. Since the observable condensate is defined as  $\langle |\Delta| \rangle$ , which is always real, we can choose it to be in real part of the diquark field. Consequently there is a  $\rho_\Delta$  in both diquark fields in the complex representation. In this case, the Goldstone mode is in the phase of the field.

The boson propagator in the real representation it is given by

$$G_\varphi = \begin{pmatrix} \frac{G_\pi}{Z_\phi} \mathbb{1}_{3 \times 3} & 0 & 0 & 0 \\ 0 & \frac{G_\sigma}{Z_\phi} & -\frac{G_{\sigma\Delta_1}}{\sqrt{Z_\phi Z_\Delta}} & -\frac{G_{\sigma\Delta_2}}{\sqrt{Z_\phi Z_\Delta}} \\ 0 & -\frac{G_{\sigma\Delta_1}}{\sqrt{Z_\phi Z_\Delta}} & \frac{G_{\Delta_1}}{Z_\Delta} & \frac{G_{\Delta_1\Delta_2}}{Z_\Delta} \\ 0 & \frac{G_{\sigma\Delta_2}}{\sqrt{Z_\phi Z_\Delta}} & -\frac{G_{\Delta_1\Delta_2}}{Z_\Delta} & \frac{G_{\Delta_2}}{Z_\Delta} \end{pmatrix}$$

with

$$G_\pi(\vec{p}^2) = K_\pi^{-1}, \quad G_\sigma(\vec{p}^2) = (K_{\Delta_1} K_{\Delta_2} + 16\mu^2 p_0^2) / J, \quad (\text{B2})$$

for the mesons and

$$G_{\Delta_1}(\vec{p}^2) = K_{\Delta_2} K_\sigma / J, \\ G_{\Delta_2}(\vec{p}^2) = (K_{\Delta_1} K_\sigma - 4\rho_\phi \rho_\Delta V_{\phi\Delta}^2) / J, \quad (\text{B3})$$

for the baryons. The indices  $\phi$  and  $\Delta$  of  $V$  denote derivatives with respect to  $\rho_\phi$  and  $\rho_\Delta$ . Further, we have the mixed contributions

$$G_{\sigma\Delta_1}(\vec{p}^2) = 2V_{\phi\Delta} \sqrt{\rho_\phi \rho_\Delta} K_{\Delta_2} / J, \\ G_{\sigma\Delta_2}(\vec{p}^2) = 8V_{\phi\Delta} \sqrt{\rho_\phi \rho_\Delta} \mu p_0 / J, \\ G_{\Delta_1\Delta_2}(\vec{p}^2) = 4\mu p_0 K_\sigma / J, \quad (\text{B4})$$

where

$$J(\vec{p}^2) = K_\sigma (K_{\Delta_1} K_{\Delta_2} + 16\mu^2 p_0^2) - 4\rho_\phi \rho_\Delta V_{\phi\Delta}^2 K_{\Delta_2}, \quad (\text{B5})$$

with

$$K_\pi(\vec{p}^2) = \vec{p}^2 + p_0^2 + V_\phi, \\ K_\sigma(\vec{p}^2) = \vec{p}^2 + p_0^2 + V_\phi + 2\rho_\phi V_{\phi\phi}, \\ K_{\Delta_1}(\vec{p}^2) = \vec{p}^2 + p_0^2 + V_\Delta + 2\rho_\Delta V_{\Delta\Delta} - 4\mu^2, \\ K_{\Delta_2}(\vec{p}^2) = \vec{p}^2 + p_0^2 + V_\Delta - 4\mu^2, \quad (\text{B6})$$

is the determinant of the  $\sigma\Delta$ -part of  $G_\varphi$  without the  $Z$ 's. We denote only space-like momentum dependencies since they will be crucial for derivations of anomalous dimensions. For the derivation of flow equations we will need derivatives of each entries of the propagators with respect to the  $K$ 's. It can be checked that

$$\frac{\partial G_{\varphi,ij}}{\partial K_{\varphi_l}} = -G_{\varphi,il} G_{\varphi,lj}. \quad (\text{B7})$$

Note that equal indices do not imply a sum in (B7). Using this relations, one can express momentum derivatives conveniently in terms of the propagators

$$\frac{\partial G_{\varphi,ij}}{\partial \vec{p}^2} = \sum_l \frac{\partial G_{\varphi,ij}}{\partial K_{\varphi_l}} = -\sum_l G_{\varphi,il} G_{\varphi,lj}. \quad (\text{B8})$$

The boson propagator in the complex representation is

$$G_{\bar{\varphi}} = \begin{pmatrix} \frac{G_\pi}{Z_\phi} \mathbb{1}_{3 \times 3} & 0 & 0 & 0 \\ 0 & \frac{G_\sigma}{Z_\phi} & \frac{G_{\sigma\Delta}^-}{\sqrt{Z_\phi Z_\Delta}} & \frac{G_{\sigma\Delta}^+}{\sqrt{Z_\phi Z_\Delta}} \\ 0 & \frac{G_{\sigma\Delta}^+}{\sqrt{Z_\phi Z_\Delta}} & \frac{G_{\Delta_1}^+}{Z_\Delta} & \frac{G_{\Delta_1\Delta_2}^+}{Z_\Delta} \\ 0 & \frac{G_{\sigma\Delta}^-}{\sqrt{Z_\phi Z_\Delta}} & \frac{G_{\Delta_1\Delta_2}^-}{Z_\Delta} & \frac{G_{\Delta_2}^-}{Z_\Delta} \end{pmatrix} \quad (\text{B9})$$

with

$$K_\Delta^\pm(\vec{p}^2) = \vec{p}^2 + (p_0 \pm 2i\mu)^2 + V_\Delta, \\ G_\Delta^\pm(\vec{p}^2) = [(K_\Delta^\mp + \rho_\Delta V_{\Delta\Delta}) K_\sigma - 2\rho_\phi \rho_\Delta V_{\phi\Delta}^2] / J, \\ G_{\Delta_1}(\vec{p}^2) = (2\rho_\phi V_{\phi\Delta}^2 - V_{\Delta\Delta} K_\sigma) \rho_\Delta / J, \\ G_{\sigma\Delta}^\pm(\vec{p}^2) = -\sqrt{2\rho_\phi \rho_\Delta} V_{\phi\Delta} K_\Delta^\mp / J. \quad (\text{B10})$$

Note that the propagator is hermitian, i.e.  $G_{\bar{\varphi},ij}^* = G_{\bar{\varphi},ji}$  and furthermore obeys  $G_{\bar{\varphi},ij}(-p_0) = G_{\bar{\varphi},ji}(p_0)$ . Since the transformation between representations affects only the diquark space,  $G_\sigma$  does not change, neither does the

determinant. The three boson vertex is given by

$$\begin{aligned}
\Gamma_{\varphi_k\varphi_j\varphi_i} = & Z_j\delta_{ji}(Z_\phi\sigma V_{\phi j}\delta_{k4} + Z_\Delta\Delta V_{j\Delta}\delta_{k5}) \\
& + Z_k\delta_{kj}(Z_\phi\sigma V_{\phi k}\delta_{i4} + Z_\Delta V_{k\Delta}\Delta\delta_{i5}) \\
& + Z_i\delta_{ik}(Z_\phi\sigma V_{\phi i}\delta_{j4} + Z_\Delta\Delta V_{i\Delta}\delta_{j5}) \\
& + (Z_\phi\sigma\delta_{k4} + Z_\Delta\Delta\delta_{k5})(Z_\phi\sigma\delta_{i4} + Z_\Delta\Delta\delta_{i5}) \\
& \times (Z_\phi\sigma\delta_{j4} + Z_\Delta\Delta\delta_{j5})V_{ijk}, \quad (\text{B11})
\end{aligned}$$

where, apart from the Kronecker delta, we apply the convention that the index is set to  $\phi$  if it corresponds to a mesonic field, and to  $\Delta$  if it corresponds to diquark field in  $\varphi$ . Accordingly  $V_{ijk}$ , where the indices denote  $\rho$ -derivatives, can either have three derivatives with respect to one species or two with respect to one and one with

respect to the other.

## 2. Fermions

It is convenient to apply the Nambu-Gorkov formalism, where the quark fields are represented by the bi-spinors in color space

$$\Psi = \begin{pmatrix} q_r \\ \tau_2 C \bar{q}_g^T \end{pmatrix}, \quad \bar{\Psi} = \begin{pmatrix} \bar{q}_r \\ q_g^T C \tau_2 \end{pmatrix}, \quad (\text{B12})$$

where the indices  $r$  and  $g$  denote the color components of the quark spinor. In the convention we apply here, the Nambu-Gorkov space is equivalent to color space. Thus we can rewrite the quark part of the effective action as  $\Gamma_q = \int_x \bar{\Psi}(x)S(x, i\partial)\Psi(x)$  with

$$S(x, i\partial) = Z_q \begin{pmatrix} i\hat{\not{p}} + i\gamma_0\mu + i\sqrt{Z_\phi}h_\phi[\sigma(x) + i\gamma_5\vec{\tau} \cdot \vec{\pi}(x)] & -\sqrt{2Z_\Delta}h_\Delta\Delta(x)\gamma_5 \\ -\sqrt{2Z_\Delta}h_\Delta\Delta^*(x)\gamma_5 & i\hat{\not{p}} - i\gamma_0\mu + i\sqrt{Z_\phi}h_\phi[\sigma(x) - i\gamma_5\vec{\tau} \cdot \vec{\pi}(x)] \end{pmatrix}. \quad (\text{B13})$$

Now we write the inverse propagator at the expansion point as

$$\begin{aligned}
G_{\bar{\Psi}\Psi}^{-1}(p) &= -[G_{\bar{\Psi}\Psi}^{-1}(-p)]^T \\
&= Z_q \begin{pmatrix} \not{p} + \gamma_0(p_0 + i\mu) + i\hat{\sigma} & -\hat{\Delta}\gamma_5 \\ -\hat{\Delta}\gamma_5 & \not{p} + \gamma_0(p_0 - i\mu) + i\hat{\sigma} \end{pmatrix}.
\end{aligned}$$

Note that if there is no tensor structure regarding a particular space (color/flavor/spinor space) an identity matrix with respect to that specific space is implied. Furthermore we choose the diquark condensate to be on the real axis. Now we invert above equation to find the Nambu-Gorkov Propagator

$$G_{\Psi\bar{\Psi}} = \frac{1}{Z_q} \begin{pmatrix} G^+ & \Delta^- \\ \Delta^+ & G^- \end{pmatrix}, \quad (\text{B14})$$

where

$$\begin{aligned}
G^\pm &= (\not{p} - i\hat{\sigma})A_\pm + \gamma_0 B_\pm, \\
\Delta^\pm &= \gamma_5 [\hat{\Delta}A \pm iF(\not{p} + i\hat{\sigma})\gamma_0]. \quad (\text{B15})
\end{aligned}$$

With  $\nu_\pm = p_0 \pm i\mu$  we define the functions as

$$\begin{aligned}
A(\vec{p}^2) &= (\vec{p}^2 + \nu_+\nu_- + \hat{\sigma}^2 + \hat{\Delta}^2)D(\vec{p}^2), \\
A_\pm(\vec{p}^2) &= (\vec{p}^2 + \nu_\mp^2 + \hat{\sigma}^2 + \hat{\Delta}^2)D(\vec{p}^2), \\
B_\pm(\vec{p}^2) &= (\nu_\pm(\vec{p}^2 + \nu_\mp^2 + \hat{\sigma}^2) + \nu_\mp\hat{\Delta}^2)D(\vec{p}^2), \quad (\text{B16})
\end{aligned}$$

and

$$F(\vec{p}^2) = 2\hat{\Delta}\mu D(\vec{p}^2), \quad D(\vec{p}^2) = \frac{1}{a_+a_- + f^2}, \quad (\text{B17})$$

where the small letter functions are the numerators of the capital letter functions. These functions have the following properties, for the sake of demonstration, we explicitly show here the  $p_0$ -dependence and omit the  $\vec{p}^2$ -dependence

$$\begin{aligned}
A(-p_0) &= A(p_0), & A_\pm(-p_0) &= A_\mp(p_0), \\
B_\pm(-p_0) &= -B_\mp(p_0), & F(-p_0) &= F(p_0), \quad (\text{B18})
\end{aligned}$$

as well as

$$A^* = A, \quad A_\pm^* = A_\mp, \quad B_\pm^* = B_\mp, \quad F^* = F. \quad (\text{B19})$$

For the flow equations, the following derivatives will be required

$$\begin{aligned}
A'_\pm &= F^2 - A_\pm^2, & A' &= D - A(A_+ + A_-), \\
B'_\pm &= \nu_\pm D - B_\pm(A_+ + A_-), & F' &= -F(A_+ + A_-), \quad (\text{B20})
\end{aligned}$$

where primes denote a derivation with respect to  $\vec{p}^2$ . Let us turn to the vertices. The quark-meson ones are given by

$$\begin{aligned}
\Gamma_{\bar{\Psi}\sigma\Psi} &= \sqrt{Z_\phi}Z_q i h_\phi \mathbf{1}, \\
\Gamma_{\bar{\Psi}\pi_i\Psi} &= \sqrt{Z_\phi}Z_q h_\phi \begin{pmatrix} -\gamma_5\tau_i & 0 \\ 0 & \gamma_5\tau_i \end{pmatrix}. \quad (\text{B21})
\end{aligned}$$

The quark-diquark vertices read

$$\begin{aligned}\Gamma_{\bar{\Psi}\Delta\Psi} &= \sqrt{2Z_\Delta}Z_q h_\Delta \begin{pmatrix} 0 & -\gamma_5 \\ 0 & 0 \end{pmatrix}, \\ \Gamma_{\bar{\Psi}\Delta^*\Psi} &= \sqrt{2Z_\Delta}Z_q h_\Delta \begin{pmatrix} 0 & 0 \\ -\gamma_5 & 0 \end{pmatrix}.\end{aligned}\quad (\text{B22})$$

In the real representation they are

$$\begin{aligned}\Gamma_{\bar{\Psi}\Delta_1\Psi} &= \sqrt{Z_\Delta}Z_q h_\Delta \begin{pmatrix} 0 & -\gamma_5 \\ -\gamma_5 & 0 \end{pmatrix} x, \\ \Gamma_{\bar{\Psi}\Delta_2\Psi} &= \sqrt{Z_\Delta}Z_q h_\Delta \begin{pmatrix} 0 & -i\gamma_5 \\ i\gamma_5 & 0 \end{pmatrix}.\end{aligned}\quad (\text{B23})$$

The unit matrix  $\mathbf{1} = \mathbf{1}_f \times \mathbf{1}_c \times \mathbf{1}_D$  is composed of a tensor product of unit matrices in color, flavor and Dirac space. Again, if there is no tensor structure regarding a particular space, an identity matrix is implied.

For completeness, we show the projection operator for the diquark Yukawa coupling we use in Sec. III F,

$$\hat{P} = \begin{pmatrix} 0 & -\gamma_5 \\ -\gamma_5 & 0 \end{pmatrix}.\quad (\text{B24})$$

It has the tensor structure of the real part of the quark-diquark vertex, since the diquark background field is real-valued.

### Appendix C: Flow equations

We employ the 3d flat regulator functions [65] for bosons and fermions

$$r_B(x) = \left(\frac{1}{x} - 1\right) \Theta(1-x),$$

$$r_F(x) = \left(\frac{1}{\sqrt{x}} - 1\right) \Theta(1-x).\quad (\text{C1})$$

The formal scale derivative acts only on the regulators

$$\tilde{\partial}_t r_B = \left[\frac{2}{x} - \eta_B \left(\frac{1}{x} - 1\right)\right] \Theta(1-x),$$

$$\tilde{\partial}_t r_F = \left[\frac{1}{\sqrt{x}} - \eta_F \left(\frac{1}{\sqrt{x}} - 1\right)\right] \Theta(1-x),\quad (\text{C2})$$

where we considered that the regulator  $R_k$  contains the wave function renormalisations. The flow equations will be displayed in terms of the following integrals, where we apply the shorthand notation  $\int_q = T \sum_n \int \frac{d^3 q}{(2\pi)^3}$ . The sum is over the Matsubara frequencies. The bosonic anomalous dimension contains two types of integrals. The first one yields the same results for bosonic and fermionic integrands

$$I_{\eta_B}^{(1)}[G, H] = \tilde{\partial}_t \frac{\partial}{\partial \bar{p}^2} \int_q G(\vec{q}_r^2) H((\vec{q} + \vec{p})_r^2) \Big|_{p=0} = \frac{k^5 T}{3\pi^2} \sum_n G'(k^2) H'(k^2).\quad (\text{C3})$$

Derivatives of fermionic functions are given in App. B 2. Bosonic derivatives can be performed with (B8). The second integral only occurs for fermionic integrands

$$\begin{aligned}I_{\eta_B}^{(2)}[G, H, m^2] &= \tilde{\partial}_t \frac{\partial}{\partial \bar{p}^2} \int_q G(\vec{q}_r^2) H((\vec{q} + \vec{p})_r^2) [\vec{q}_r \cdot (\vec{q} + \vec{p})_r + m^2] \Big|_{p=0} \\ &= \frac{k^3 T}{3\pi^2} \sum_n \left[ k^2 (k^2 + m^2) G'(k^2) H'(k^2) - \frac{G(k^2) H(k^2)}{4} - (1 - \eta) G(k^2) \left( \frac{H(k^2)}{2} + k^2 H'(k^2) \right) \right].\end{aligned}\quad (\text{C4})$$

This is only valid for one single fermionic species. Fermionic self-energy diagrams contain mixed integrals

$$I_{\eta_F}[G_F, H_B] = -\tilde{\partial}_t \frac{\partial}{\partial \bar{p}^2} \cdot \int_q \vec{q}(1 + r_F(\vec{q}^2)) G_F(\vec{q}_r^2) H_B((\vec{q} - \vec{p})_r^2) \Big|_{p=0} = -\frac{k^5 T}{\pi^2} \sum_n G_F(k^2) \sum_i \left(1 - \frac{\eta_{\varphi_i}}{4}\right) \frac{\partial H_B(k^2)}{\partial K_{\varphi_i}(k^2)}.\quad (\text{C5})$$

The second sum is over all bosonic species and  $K_{\varphi_i}$  represents the functions given in App. B 1 in particular (B7) can be used. And finally

$$I_h[G_F, H_B] = -\tilde{\partial}_t \int_q G_F(\vec{q}_r^2) H_B(\vec{q}_r^2) = -\frac{k^5 T}{3\pi^2} \sum_n \left[ G_F(k^2) \sum_i \left(1 - \frac{\eta_{\varphi_i}}{4}\right) \frac{\partial H_B(k^2)}{\partial K_{\varphi_i}(k^2)} + \left(1 - \frac{\eta_F}{4}\right) H_B(k^2) G_F'(k^2) \right].\quad (\text{C6})$$

Now can we write down all flow equations in terms of the above integrals. The anomalous dimensions are

$$\begin{aligned}
\eta_\phi &= 2I_{\eta_B}^{(1)} [G_\pi, \rho_\phi V_{\phi\phi}^2 G_\sigma + \rho_\Delta V_{\phi\Delta}^2 G_{\Delta_1} - 2\sqrt{\rho_\phi\rho_\Delta} V_{\phi\phi} V_{\phi\Delta} G_{\sigma\Delta_1}] \\
&\quad + 4N_c N_f h_\phi^2 \left\{ I_{\eta_B}^{(2)} [A_+, A_+, \hat{\sigma}^2] + I_{\eta_B}^{(1)} [B_+, B_+] + \hat{\Delta}^2 I_{\eta_B}^{(1)} [A, A] - I_{\eta_B}^{(2)} [F, F, \hat{\sigma}^2] \right\}, \\
\eta_\Delta &= 2I_{\eta_B}^{(1)} [G_{\Delta_2}, \rho_\Delta V_{\Delta\Delta}^2 G_{\Delta_1} + \rho_\phi V_{\phi\Delta}^2 G_\sigma - 2\sqrt{\rho_\phi\rho_\Delta} V_{\Delta\Delta} V_{\phi\Delta} G_{\sigma\Delta_1}] + 2\rho_\phi V_{\phi\Delta}^2 I_{\eta_B}^{(1)} [G_{\sigma\Delta_2}, G_{\sigma\Delta_2}] \\
&\quad + 2\rho_\Delta V_{\Delta\Delta}^2 I_{\eta_B}^{(1)} [G_{\Delta_1\Delta_2}, G_{\Delta_1\Delta_2}] - 4\sqrt{\rho_\phi\rho_\Delta} V_{\Delta\Delta} V_{\phi\Delta} I_{\eta_B}^{(1)} [G_{\sigma\Delta_2}, G_{\Delta_1\Delta_2}] \\
&\quad + 4N_c N_f h_\Delta^2 \left\{ I_{\eta_B}^{(2)} [A_-, A_+, \hat{\sigma}^2] + I_{\eta_B}^{(1)} [B_-, B_+] + \hat{\Delta}^2 I_{\eta_B}^{(1)} [A, A] + I_{\eta_B}^{(2)} [F, F, \hat{\sigma}^2] \right\}, \\
\eta_q &= \frac{1}{3} h_\phi^2 \text{Re } I_{\eta_F} [A_+, 3G_\pi + G_\sigma] + \frac{2}{3} h_\Delta^2 \text{Re } I_{\eta_F} [A_+, G_\Delta^+]. \tag{C7}
\end{aligned}$$

We note that, at finite temperature, the components of the wave function renormalisations parallel,  $Z^\parallel$ , and perpendicular,  $Z^\perp$ , to the heat bath are different a priori. However, at scales above the temperature scale,  $T/k < 1$ , the system is insensitive to thermal effects. On the other hand, for  $T/k \gg 1$  the finite temperature RG flow is only driven by the lowest Matsubara mode. While it is zero for bosons and  $Z^\parallel$  drops out, it is proportional to  $T$  for fermions which therefore decouple in this regime. Hence, we used the approximation  $Z^\parallel \equiv Z$ . Finally, the flow equations of the Yukawa couplings are

$$\begin{aligned}
\partial_t h_\phi &= \left( \eta_q + \frac{\eta_\phi}{2} \right) h_\phi + h_\phi \text{Re} \left\{ h_\phi^2 I_h [A_+, 3G_\pi(q) - G_\sigma(q)] + 2h_\Delta^2 I_h [A_+, G_\Delta^+] \right\}, \\
\partial_t h_\Delta &= \left( \eta_q + \frac{\eta_\Delta}{2} \right) h_\Delta + h_\Delta \text{Re} \left\{ h_\phi^2 I_h [A, 3G_\pi(q) + G_\sigma(q)] - 2h_\Delta^2 I_h [A, G_{|\Delta|}] - 2\frac{h_\phi^2 \sigma}{\Delta} I_h [A_+, G_{\sigma\Delta}^+] \right\}. \tag{C8}
\end{aligned}$$

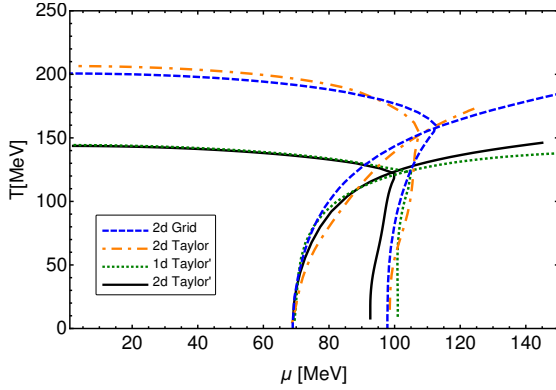


Figure 14: A comparison between various phase diagrams obtained from different truncations with the FRG. We want to emphasise that there is only a small difference between the one-dimensional Taylor expansion (dotted green line) and the two-dimensional Taylor expansion (solid black line).

#### Appendix D: One-dimensional Taylor expansion

We mentioned in Sec. III D that with a one-dimensional expansion of the effective potential in terms of the  $SO(6)$ -invariant  $\rho = \rho_\phi + \rho_\Delta$  the violation of the Silver Blaze property for an expansion scheme in terms of momentum independent meson-diquark correlation functions can be

avoided. The reason is that the  $SO(6)$  flavor symmetry relates all  $2n$ -meson- $2m$ -diquark interactions  $\lambda_{n,m}$  to purely mesonic interactions,  $\lambda_{n,m} = \lambda_{n+m,0}$ . Hence, all  $n$ -point functions that involve baryons can be defined purely in terms of mesons. This bypasses the necessity to consider frequency dependent couplings.

This construction assumes a larger flavor symmetry than the system has at finite density. It is nonetheless instructive to consider the one-dimensional expansion since technically less demanding than the two-dimensional expansion. Furthermore, it allowed us to explicit confirm our statements concerning the Silver Blaze property. Thus, we will provide the parameterisations as well as a set of initial conditions for the one-dimensional Taylor expansion here.

In the normal phase with  $\rho_\Delta = 0$  we parametrise the effective potential as

$$V_{nor}(\rho) = m^2 \rho + \sum_{n=2}^N \frac{\lambda_n}{n!} (\rho - \kappa)^n, \tag{D1}$$

where  $\kappa = \kappa_\phi + \kappa_\Delta$  and we dropped irrelevant constant. With this Ansatz the derivative terms in (21) reduce to  $V'_{nor}(\kappa) = m^2$  and the solution is given by

$$\kappa_\phi = \frac{1}{2} \left( \frac{c}{m^2} \right)^2, \quad \kappa_\Delta = 0. \tag{D2}$$

Note that this solution is only valid away from the chiral limit  $c=0$ . For the effective potential to have a minimum,

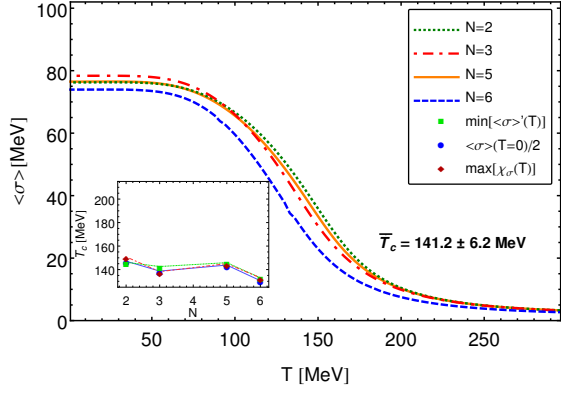


Figure 15: Chiral condensate over temperature as well as the transition temperatures at  $\mu = 0$  for various orders of the expansion of the effective potential.

the determinant of the Hessian matrix needs to be larger than zero,

$$\det \left( \frac{\partial^2 U}{\partial \varphi_i \partial \varphi_j} \right) \Big|_{\rho=\kappa} = (m^2)^{N_\phi} (m^2 - 4\mu^2)^{N_\Delta} > 0 \quad (\text{D3})$$

where  $\varphi_i$  represents the real-valued components of the boson field (see App. B 1), and  $N_\phi, N_\Delta$  are the number of meson and diquark fields respectively. As long as  $m^2 > 4\mu^2$  we are in the normal regime. At  $m^2 = 4\mu^2$  the diquark curvature mass vanishes. This indicates a second order phase transition to the BEC phase and spontaneous breaking of  $U(1)_B$  symmetry. For  $m^2 < 4\mu^2$  we use the parametrisation discussed below.

Since  $m$  is the mass of the pions, diquark condensation sets in when the quark chemical potential reaches half of the pion mass. The latter is, according to the Silver Blaze property, independent of the chemical potential at  $T = 0$ . Hence, if the Silver Blaze property is not violated,  $\mu_c = m_\pi/2$  holds within the 1d-Taylor expansion Ansatz. We will elaborate on this in Sec. II C.

For the BEC phase we reparameterise the potential by renaming  $m^2 = \lambda_2(\kappa - v)$ , thus we exchange  $m$  in favor of  $v$  and write (by adding an irrelevant constant)

$$V_{bec}(\rho) = \frac{\lambda_2}{2}(\rho - v)^2 + \sum_{n=3}^N \frac{\lambda_n}{n!}(\rho - \kappa)^n. \quad (\text{D4})$$

In this parametrisation we have  $V'_{bec}(\kappa) = \lambda_2(\kappa - v)$ , and (21) now yields

$$\kappa_\phi = \frac{1}{2} \left( \frac{c}{4\mu^2} \right)^2, \quad \kappa_\Delta = v + \frac{4\mu^2}{\lambda_2} - \frac{1}{2} \left( \frac{c}{4\mu^2} \right)^2. \quad (\text{D5})$$

We see that the chiral order parameter  $\sigma_0 = \sqrt{2\kappa_\phi}$  is proportional to  $\mu^{-2}$ . Furthermore, with rising  $\mu$  the ground state rotates from the mesonic direction to the diquark direction.

Furthermore, we set  $h_\Delta = h_\phi$ , and following our discussion above, the flows of all Taylor coefficients are given by the mesonic ones. However, the wave function renormalisations of mesons and diquarks are independent. For the UV cutoff  $\Lambda = 900 \text{ MeV}$  we used as initial parameters  $\langle \sigma \rangle_\Lambda = 2.28 \text{ MeV}$ ,  $m_{\phi,\Lambda} = 1090 \text{ MeV}$ ,  $\lambda_{2,\Lambda} = 89$  and  $h_{\phi,\Lambda} = 6.3$ . These initial conditions give a constituent quark mass of  $360 \text{ MeV}$ ,  $m_\pi = 139 \text{ MeV}$  as well as  $f_\pi = 76 \text{ MeV}$  in the IR. Since Silver Blaze is fulfilled by construction in this case, the latter exactly determines the onset chemical potential, i.e.  $m_\pi = 2\mu_c$ .

The resulting phase diagram is shown in Fig. 14. Remarkably, there is only a small difference between the two-dimensional expansion (solid black line) and the one-dimensional expansion (dotted green line). Hence, the dynamics of QC<sub>2</sub>D are mainly driven by the mesons, also at high density. This may be the most striking difference between QC<sub>2</sub>D and QCD but has yet to be explored.

Finally, we discuss the convergence of the 1d Taylor expansion. In Fig. 15 we show the chiral condensate as a function of the temperature for different orders  $N$  of the Taylor expansion. All curves are computed with the same UV initial conditions as specified above. We see that the expansion does not converge for the orders we have computed. The crossover temperature has been computed with three different definitions as shown in the legend of Fig. 15. As a function of the order  $N$  the critical temperature does not converge as well. Therefore the average  $\bar{T}_c$  computed from the arithmetic mean of all three definitions of  $t_c$  and all orders, together with its margin of error, should give a feeling for the error of our phase boundaries.

In Ref. [45] a Taylor expansion with a fixed expansion point, rather than a co-moving minimum, was employed for a quark-meson model. There, a rapid convergence of the expansion was observed for all temperature regions. As it was discussed there, the back-coupling of higher order couplings into the flow equations at lower orders in the co-moving expansion is responsible for numerical instabilities and slow convergence. Hence, in light of these findings, the lack of convergence in the present work is no surprise.

[1] P. Braun-Munzinger and J. Wambach, Rev. Mod. Phys. **81**, 1031 (2009).

[2] J. Kogut, M. A. Stephanov, and D. Toublan, Phys.Lett.

- B464**, 183 (1999), hep-ph/9906346.
- [3] J. Kogut, M. A. Stephanov, D. Toublan, J. Verbaarschot, and A. Zhitnitsky, Nucl.Phys. **B582**, 477 (2000), hep-ph/0001171.
- [4] K. Splittorff, D. Son, and M. A. Stephanov, Phys.Rev. **D64**, 016003 (2001), hep-ph/0012274.
- [5] K. Splittorff, D. Toublan, and J. Verbaarschot, Nucl.Phys. **B620**, 290 (2002), hep-ph/0108040.
- [6] G. V. Dunne and S. M. Nishigaki, Nucl.Phys. **B654**, 445 (2003), hep-ph/0210219.
- [7] G. V. Dunne and S. M. Nishigaki, Nucl.Phys. **B670**, 307 (2003), hep-ph/0306220.
- [8] T. Brauner, Mod.Phys.Lett. **A21**, 559 (2006), hep-ph/0601010.
- [9] T. Kanazawa, T. Wettig, and N. Yamamoto, JHEP **0908**, 003 (2009), 0906.3579.
- [10] T. Kanazawa, T. Wettig, and N. Yamamoto, Phys.Rev. **D81**, 081701 (2010), 0912.4999.
- [11] L. Kondratyuk, M. Giannini, and M. Krivoruchenko, Phys.Lett. **B269**, 139 (1991).
- [12] R. Rapp, T. Schaefer, E. V. Shuryak, and M. Velkovsky, Phys.Rev.Lett. **81**, 53 (1998), hep-ph/9711396.
- [13] C. Ratti and W. Weise, Phys.Rev. **D70**, 054013 (2004), hep-ph/0406159.
- [14] G.-f. Sun, L. He, and P. Zhuang, Phys.Rev. **D75**, 096004 (2007), hep-ph/0703159.
- [15] T. Brauner, K. Fukushima, and Y. Hidaka, Phys.Rev. **D80**, 074035 (2009), 0907.4905.
- [16] J. O. Andersen and T. Brauner, Phys.Rev. **D81**, 096004 (2010), 1001.5168.
- [17] M. Harada, C. Nonaka, and T. Yamaoka, Phys.Rev. **D81**, 096003 (2010), 1002.4705.
- [18] T. Zhang, T. Brauner, and D. H. Rischke, JHEP **1006**, 064 (2010), 1005.2928.
- [19] S. Imai, H. Toki, and W. Weise (2012), 1210.1307.
- [20] L. He, Phys. Rev. **D82**, 096003 (2010), 1007.1920.
- [21] A. Nakamura, Phys.Lett. **B149**, 391 (1984).
- [22] S. Hands, J. B. Kogut, M.-P. Lombardo, and S. E. Morrison, Nucl.Phys. **B558**, 327 (1999), hep-lat/9902034.
- [23] S. Hands, I. Montvay, S. Morrison, M. Oevers, L. Scorzato, et al., Eur.Phys.J. **C17**, 285 (2000), hep-lat/0006018.
- [24] S. Hands, I. Montvay, L. Scorzato, and J. Skullerud, Eur.Phys.J. **C22**, 451 (2001), hep-lat/0109029.
- [25] S. Muroya, A. Nakamura, and C. Nonaka, Nucl.Phys.Proc.Suppl. **119**, 544 (2003), hep-lat/0208006.
- [26] S. Chandrasekharan and F.-J. Jiang, Phys.Rev. **D74**, 014506 (2006), hep-lat/0602031.
- [27] S. Hands, S. Kim, and J.-I. Skullerud, Eur. Phys. J. **C48**, 193 (2006), hep-lat/0604004.
- [28] S. Hands, P. Kenny, S. Kim, and J.-I. Skullerud, Eur.Phys.J. **A47**, 60 (2011), 1101.4961.
- [29] S. Cotter, P. Giudice, S. Hands, and J.-I. Skullerud, Phys.Rev. **D87**, 034507 (2013), 1210.4496.
- [30] S. Hands, S. Kim, and J.-I. Skullerud, Phys.Lett. **B711**, 199 (2012), 1202.4353.
- [31] T. Boz, S. Cotter, L. Fister, D. Mehta, and J.-I. Skullerud (2013), 1303.3223.
- [32] P. Scior and L. von Smekal (2015), 1508.00431.
- [33] N. Strodthoff, B.-J. Schaefer, and L. von Smekal, Phys.Rev. **D85**, 074007 (2012), 1112.5401.
- [34] D. F. Litim and J. M. Pawłowski, in *The exact renormalization group. Proceedings, Workshop, Faro, Portugal, September 10-12, 1998* (1998), pp. 168–185, hep-th/9901063, URL <http://alice.cern.ch/format/showfull?sysnb=0302190>.
- [35] J. Berges, N. Tetradis, and C. Wetterich, Phys. Rept. **363**, 223 (2002), hep-ph/0005122.
- [36] J. Polonyi, Central Eur. J. Phys. **1**, 1 (2003), hep-th/0110026.
- [37] J. M. Pawłowski, Annals Phys. **322**, 2831 (2007), hep-th/0512261.
- [38] H. Gies, Lect.Notes Phys. **852**, 287 (2012), hep-ph/0611146.
- [39] B.-J. Schaefer and J. Wambach, Phys.Part.Nucl. **39**, 1025 (2008), hep-ph/0611191.
- [40] O. J. Rosten, Phys. Rept. **511**, 177 (2012), 1003.1366.
- [41] J. Braun, J. Phys. **G39**, 033001 (2012), 1108.4449.
- [42] L. von Smekal, Nucl.Phys.Proc.Suppl. **228**, 179 (2012), 1205.4205.
- [43] J. M. Pawłowski, Nucl.Phys. **A931**, 113 (2014).
- [44] N. Strodthoff and L. von Smekal, Phys. Lett. **B731**, 350 (2014), 1306.2897.
- [45] J. M. Pawłowski and F. Rennecke, Phys. Rev. **D90**, 076002 (2014), 1403.1179.
- [46] S. Diehl, H. Gies, J. Pawłowski, and C. Wetterich, Phys.Rev. **A76**, 053627 (2007), cond-mat/0703366.
- [47] S. Diehl, S. Floerchinger, H. Gies, J. Pawłowski, and C. Wetterich, Annalen Phys. **522**, 615 (2010), 0907.2193.
- [48] S. Floerchinger, M. Scherer, S. Diehl, and C. Wetterich, Phys.Rev. **B78**, 174528 (2008), 0808.0150.
- [49] S. Floerchinger, M. Scherer, and C. Wetterich, Phys.Rev. **A81**, 063619 (2010), 0912.4050.
- [50] M. M. Scherer, S. Floerchinger, and H. Gies, Phil. Trans. Roy. Soc. Lond. **A368**, 2779 (2011), 1010.2890.
- [51] I. Boettcher, J. M. Pawłowski, and S. Diehl, Nucl.Phys.Proc.Suppl. **228**, 63 (2012), 1204.4394.
- [52] D. Schnoerr, I. Boettcher, J. M. Pawłowski, and C. Wetterich (2013), 1301.4169.
- [53] H. Gies and C. Wetterich, Phys.Rev. **D65**, 065001 (2002), hep-th/0107221.
- [54] S. Floerchinger and C. Wetterich, Phys.Lett. **B680**, 371 (2009), 0905.0915.
- [55] J. Braun, L. Fister, J. M. Pawłowski, and F. Rennecke (2014), 1412.1045.
- [56] M. Mitter, J. M. Pawłowski, and N. Strodthoff, Phys. Rev. **D91**, 054035 (2015), 1411.7978.
- [57] C. Wetterich, Phys.Lett. **B301**, 90 (1993).
- [58] T. D. Cohen, Phys. Rev. Lett. **91**, 222001 (2003), hep-ph/0307089.
- [59] G. Markó, U. Reinosa, and Z. Szép, Phys. Rev. D **90**, 125021 (2014).
- [60] A. J. Helmboldt, J. M. Pawłowski, and N. Strodthoff, Phys. Rev. **D91**, 054010 (2015), 1409.8414.
- [61] W.-j. Fu and J. M. Pawłowski (2015), 1508.06504.
- [62] A. Eichhorn, D. Mesterházy, and M. M. Scherer, Physical Review E **88**, 042141 (2013).
- [63] L. Classen, I. F. Herbut, L. Janssen, and M. M. Scherer, arXiv preprint arXiv:1510.09003 (2015).
- [64] F. Rennecke, Phys. Rev. D **92**, 076012 (2015), 1504.03585.
- [65] D. F. Litim, Phys.Rev. **D64**, 105007 (2001), hep-th/0103195.